

POLITECNICO DI TORINO

Master's Degree in Green building Engineering



**Politecnico
di Torino**

Master's Degree Thesis

Shallow tunneling in Bimrocks

Supervisors

Prof. Monica Barbero

Dr. Maria Lia Napoli

Candidate

Masoud Ghasoddin

March 2025

Summary

Shallow tunneling within block-in-matrix rocks (Bimrocks) poses considerable geotechnical challenges due to their varied composition and unpredictable mechanical properties. This thesis explores the behavior of shallow tunnels situated in bimrocks, with a particular emphasis on how the Volumetric Block Proportion (VBP) influences tunnel stability and surface displacement.

A detailed numerical analysis was performed utilizing RS2 modeling, which examined different VBP scenarios (25%, 40%, 55%) to evaluate deformation characteristics. The research incorporates stochastic modeling techniques to replicate the random distribution of rock blocks, thereby providing an accurate depiction of bimrock formations.

The findings demonstrate that an increase in VBP contributes to enhanced tunnel stability by mitigating surface settlement and deformation, with a notable 62.16% reduction in vertical displacement as VBP escalates from 0% to 55%. Conversely, the Von Mises stress exhibits an upward trend with higher VBP levels, attributed to the redistribution of stress around rigid blocks. The research identifies 40% VBP as the worst point for achieving maximum shear strain, where stress concentration and deformation are most significant. These results underscore the necessity of accounting for bimrock heterogeneity in geotechnical design, especially in the context of urban tunneling initiatives.

Future investigations should focus on aspects such as block size distribution, anisotropy, and the effects of dynamic loading to further refine predictive models and advance tunneling practices in intricate geological environments.

Acknowledgements

I wish to convey my heartfelt appreciation to my wife, Marziyeh, for her steadfast love, patience, and unwavering support during this journey. Her faith in my abilities and her numerous sacrifices have provided me with immense strength; this thesis would not have been achievable without her.

I am equally thankful to my supervisor, Prof. Monica Barbero, for her committed support and invaluable guidance throughout my research. Her expertise, patience, and encouragement have been crucial in the development of this work.

I extend my special thanks to my co-supervisor, Dr. Maria Lia Napoli, for her insightful comments, thoughtful recommendations, and ongoing encouragement. Her feedback on the writing of this thesis has been incredibly beneficial and has significantly improved the quality of this work.

I appreciate all of you for being integral to this achievement.

Contents

1. Bimrocks	3
1. Bimrocks	4
1.1. General Description	4
1.2. Bimrock identification challenges	8
1.3. Bimrocks Characteristics	10
1.3.1. Block size distribution	10
1.3.2. The Concepts of Self Similarity and Fractal Dimension	11
1.3.3. Block-matrix threshold	15
1.3.4. Volumetric Block Proportion (VBP)	16
1.3.4.1. Estimating VBP	16
1.4. Mechanical characteristics of Bimrocks	22
2. Tunneling	32
2. Benefits from tunneling	33
2.1. Tunnel construction techniques	33
2.1.1. Conventional Methods	33
2.2. Full face mechanized Methods and improvement's techniques	33
2.3. Stability problems in tunneling.....	35
2.3.1. Deep tunnels.....	35

2.3.2.	Shallow tunnels.....	38
3.	Numerical Modeling.....	44
3.	Analysis of Shallow Tunneling in Bimrocks.....	45
3.1.	Numerical models arrangements.....	45
3.2.	Material properties.....	46
3.3.	RS2 Modeling.....	47
3.4.	Results.....	52
3.4.1.	Vertical displacement.....	52
3.4.2.	Yielded elements.....	57
3.4.3.	Maximum shear strain.....	58
3.4.4.	Von Mises Stress.....	61
3.5.	Conclusion.....	64
	Bibliography.....	65
	Appendix.....	72

List of figures

Figure 1-1 Character and classification of melanges and related rock bodies (Raymond, 1984)	5
Figure 1-2 Global Distribution of Mélange and Ophiolites (Medley, 1994).....	6
Figure 1-3 Some samples and outcrops of typical bimrocks a) (Coli, et al., 2011), b) (Afifipour, et al., 2014).....	7
Figure 1-4 Rock Mass in Bimrock formation (The dashed line on the map shows the planned area for the road cut) (Medley, 1999)	9
Figure 1-5 The impact of block size distribution on the "roughness" of failure surfaces was examined for two different distributions having the same block volumetric proportion (Lindquist, 1994).....	11
Figure 1-6 The disorder of Franciscan melange exposed at a road cut (Medley, 1994).	12
Figure 1-7 Franciscan mélange outcrop at Caspar Headlands, Mendocino County, Northern California, displaying the dmod: maximum observed dimension (Medley, et al., 1995).	13
Figure 1-8 Log-log histograms for two distinct areas (Medley, 1994).....	14
Figure 1-9 Compilation of log-histograms for the block sizes of 1,900 blocks in Franciscan mélanges, with sizes ranging from millimeters to kilometers(Medley, 1994).	15
Figure 1-10 sketch illustrating different scales of interest for an area and the concept of block/matrix threshold, with the right side labeled "Road Width 20m." (Medley, 2001).	16

Figure 1-11 (a) Core Analysis (Medley, 2001), (b) Image analysis (Lindquist, et al., 1994), 32%VBP virtual bimrock model with example virtual borings (dimensions in millimeters) (Napoli, et al., 2022)..... 19

Figure 1-12 The 3D block size distribution is only marginally replicated by the 1D chord distribution. 1D chord overestimates the smaller diameters and underestimates the bigger block size (Medley, 2001) s..... 20

Figure 1-13 Uncertainty in the estimated values of VBP in relation to the measured linear block proportion (13 to 55%) and the length of linear measurement (LBP), which is expressed as a multiple (N) of the length of the biggest block (dmax) (Medely, 1997). 21

Figure 1-14 A comparison of the 1D chord length distributions and the 3D block size distributions (3D BSD and 3D CLD) (Medley, 2001)..... 22

Figure 1-15 The influence of block volumetric proportion on the cohesion and friction angle of physical model mélanges was assessed through triaxial compression tests on 150 mm diameter specimens (Lindquist, 1994)..... 23

Figure 1-16 rising trend in the friction angle in different investigations studies (Lindquist, 1994)..... 23

Figure 1-17 manufactured specimens of bimrocks by four different block orientations . (Lindquist, 1994)..... 24

Figure 1-18 Comparing VBP and UCS changes in present and previous studies (Hu, et al., 2024). 25

Figure 1-19 the stages involved in sampling: (a) a synthetic block-in-matrix mixture prior to being poured into the mold, (b) a standard molded mixture, (c) six representative cylindrical bimrock samples, (d) a cylindrical sample following the

molding of the initial half, (e) the process of molding the second half, and (f) the removal of the completed sample from the mold (Yazdani, et al., 2024)..... 26

Figure 1-20 Correlation between BF and VBP (Yazdani, et al., 2024). 27

Figure 1-21 (a) Main section of the Nuozhandu embankment dam, (b) The relationship between shear strength and normal stress of the test samples (Zhang, et al., 2016).... 29

Figure 1-22 Impact of the (VBP) on bimrock specimens' (a) unconfined compressive strength and (b) average deformation modulus (Barbero, et al., 2008). 30

Figure 1-23 Failure of the bimrock specimens with VBP of 75% under various strain rates (Sharafisafa, et al., 2024)..... 31

Figure 2-1 The Klang Valley multimode tunnel boring machine (TBM) features a diameter of 6.62 meters. (a) the TBM cutterhead is depicted within the factory, the excavation chamber (plenum) and the terminal section of the screw conveyor. (b) the TBM is illustrated upon the completion of a drive, highlighting the geological material it is penetrating. (c) the TBM is shown operating in Earth Balance Mode (EBM). (d) the TBM is represented in slurry mode, with visible connections for the slurry line. (Image credit: Herrenknecht.), (Chapman, et al., 2018). 34

Figure 2-5 Layout of reinforcement scheme-1 of tunnel bottom (unit: mm), (Zhou, et al., 2014). 36

Figure 2-3 (a) Example of a modified rock mass in bimrock including a homogeneous outer layer,(b) An example of the final geometry, (c) A 70% VBP bimrock model with the tunnel indicated by a red circle is shown on the left. A close-up of the mesh created for the block-in-matrix area of the same bimrock model is shown on the right (Napoli, et al., 2021). 37

Figure 2-4 Modes of deformation and symbols for shallow tunnel (Pinto, et al., 2013)	39
Figure 2-5 Schematic illustration of the numerical model (unit: m), (Patil, et al., 2018)	40
Figure 2-6 (a) Joint model, boundary conditions and the geometry of a horseshoe tunnel, (b) normal stresses along joints at distance ranges of ± 2.5 m from the centre of the tunnel , (R. Abdellah, et al., 2018)	41
Figure 2-7 (a) Surface settlement in existing building loads: D/B = 2.0 (shallow tunneling), (b) Surface settlement in existing building loads: D/B = 4.0 (deep tunneling), (Shahin, et al., 2016)	42
Figure 2-8 station 1,779 south bore Spital tunnel; displacements in a block impacted by the monitored displacements. Changes are amplified by 25 (Button, et al., 2004)	43
Figure 3-1 Example of different block arrangements for VBP in the range 25%-55%. The tunnel is represented by the red circle.	46
Figure 3-2 Numerical model dimensions (dimensions are in meters)	47
Figure 3-3 Defined Stages	48
Figure 3-4 Define material properties	49
Figure 3-5 Field stress properties	49
Figure 3-6 Mesh setup	50
Figure 3-7 The final modeling: (a) before excavation, (b) first stage of excavation	51
Figure 3-8 vertical displacement on the ground Surface (m), Matrix-only	52
Figure 3-9 vertical displacement on the ground Surface (m), VBP 25%	53
Figure 3-10 vertical displacement on the ground Surface (m), VBP 40%	54
Figure 3-11 vertical displacement on the ground Surface (m), VBP 55%	55

Figure 3-12 vertical displacement versus VBP %	56
Figure 3-13 Yielded elements.....	57
Figure 3-14 Maximum shear strain.....	60
Figure 3-15 Von Mises Stress.....	63
Appendix.....	72

List of tables

Table 3-1 Designated Material Characteristics.....	46
Table 3-2 Defined Stages.....	48
Table 3-3 Maximum displacement and it's variations in different models	56

Introduction

Tunneling within heterogeneous geological formations poses considerable challenges due to the intricate mechanical properties of the ground. A particularly problematic material in this context is Block-in-Matrix Rock (Bimrock), which is characterized by a weaker matrix interspersed with randomly oriented rigid blocks. The erratic distribution and interaction of these elements lead to significant engineering obstacles, especially in shallow tunneling scenarios where ground deformation and stability are paramount. A critical factor affecting the mechanical behavior of Bimrocks is the Volumetric Block Proportion (VBP), which quantifies the ratio of blocks to the matrix. It is crucial to comprehend how varying levels of VBP influence tunnel stability, stress distribution, and surface settlement to ensure the design of safe and effective underground structures. This dissertation examines the impact of VBP on the behavior of shallow tunneling through numerical simulations utilizing RS2 (Finite Element Method). Different VBP scenarios (0%, 25%, 40%, and 55%) are evaluated to investigate ground deformation, stress redistribution, and yielded elements. The results are intended to offer significant insights into the geotechnical design considerations for tunnels situated in Bimrock formations, particularly in urban and infrastructure developments where maintaining surface stability is of utmost importance.

Chapter 1 provides a general introduction to Bimrocks and their significance in geotechnical engineering. It discusses key characteristics such as rock block distribution, scale independence, VBP estimation, and related uncertainties. Additionally, various literature studies on the mechanical properties and behavior of Bimrocks are reviewed.

Chapter 2 focuses on tunneling, providing an overview of construction techniques while assessing the stability challenges associated with both shallow and deep tunnels.

Chapter 3 delineates the numerical modeling strategy employed in this research. It elaborates on the configuration of the model, the characteristics of the materials, the boundary conditions, and the stages of excavation. Furthermore, it examines both homogeneous and heterogeneous methodologies applied in the analysis of tunnel stability, citing significant techniques from earlier investigations. The chapter also presents the outcomes and interpretations of the numerical simulations, focusing on

vertical displacement, stress distribution, shear strain, and yielding elements across various VBP configurations. The results are corroborated by comparisons with prior research. In conclusion, the chapter encapsulates the principal findings and implications of the study.

1. Bimrocks

1. Bimrocks

1.1. General Description

Many geologic processes produce block-in-matrix rocks, and a partial list could include: sedimentary rocks (boulder conglomerates, lithified colluvium and talus, and tillites); igneous volcanic rocks (agglomerates, pyroclastics, lahars, xenolithic inclusions in volcanic extrusions); plutonic rocks (xenolithic inclusions in igneous intrusions); structural brittle cataclastics (fault breccias); rocks formed by structural ductile deformation on the interference zones of folds (mylonites); rocks formed by diapirism (some sheared serpentinites) and rocks formed by chemical and mechanical weathering (saprolites, decomposed granites, cemented colluvium) (Medley, 1994).

(Raymond, 1984) provided a schematic diagram that depicts the character and classification of melanges and similar heterogeneous rock bodies. Figure 1-1 shows a continuum of progressive fragmentation and mixing of interbedded sandstone/shale sequences, divided into four types of units: α , β , γ , and δ . Figure 1-1 also shows the progressive fragmentation and mixing of a protolithic rock type into a fragmented unit derived from another protolith. Finally, the diagram presents eight possible classes of melanges and related rock bodies, based on their origin (igneous, sedimentary, or tectonic) and genetic type (polygenetic).

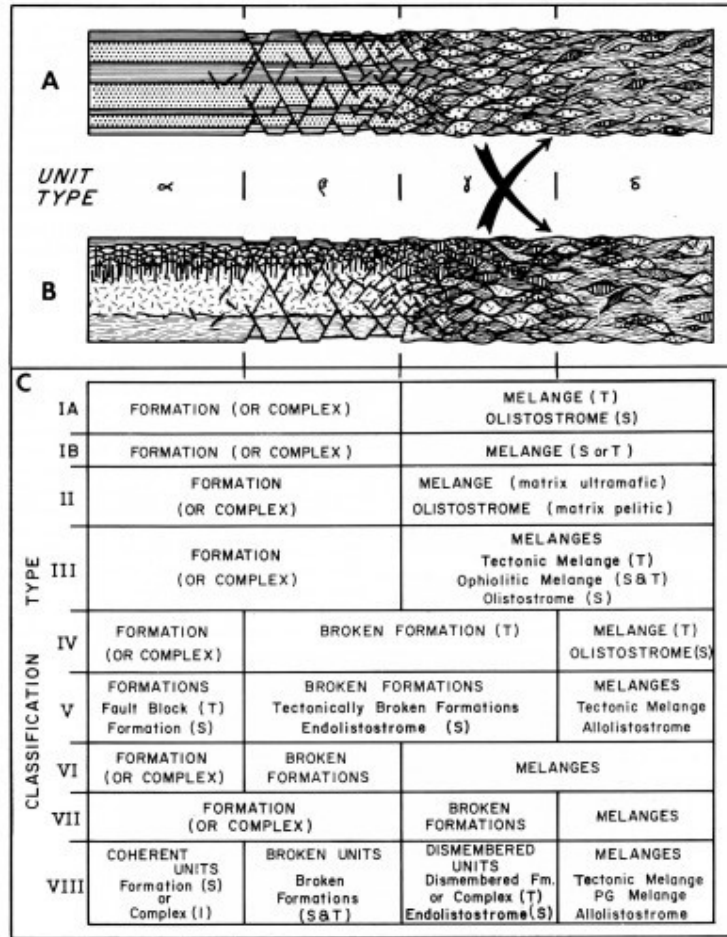


Figure 1-1 Character and classification of melanges and related rock bodies (Raymond, 1984)

(Raymond, 1984) categorized melanges, opisthosomas, and other complex geological formations as "Block-In-Matrix" formations.

The Raymond's term "Blocks In Matrix" was shortened to "bimrocks" (which stands for "block-in-matrix rocks") by (Medley, 1994), to describe rock masses composed of large chunks embedded in a finer material. These types of rocks are often found in complex formation like melanges and fault zones. The presence of these larger chunks affects the overall mechanical behavior of the rock, making it important to consider in geological and engineering studies. (Medley, 1994) came up with the term "bimsoil" to describe geological units that have pieces of rock embedded in a soil-like material (Kalender, et al., 2014). Bimrocks and Bimsoils can be found in approximately 60 countries, including the United States, Italy, Turkey, and Iran (Medley, 1994).

Figure 1-2 shows the worldwide distribution of Mélange and Ophiolites and Figure 1-3 gives some examples of bimrocks.

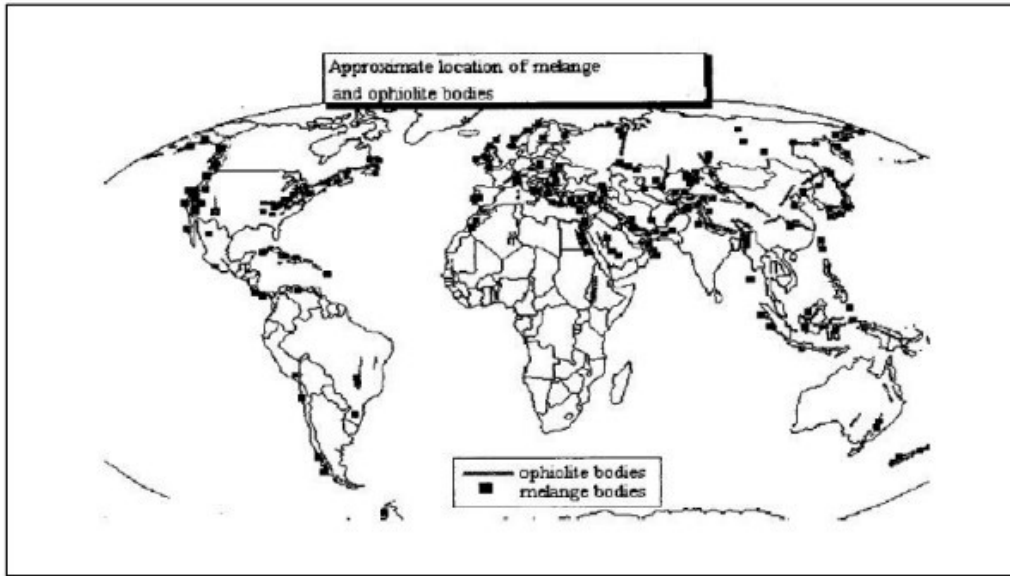


Figure 1-2 Global Distribution of Mélange and Ophiolites (Medley, 1994)

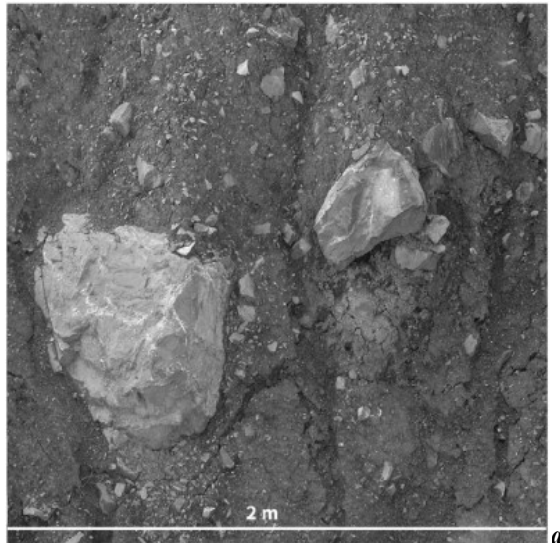




Figure 1-3 Some samples and outcrops of typical bimrocks a) (Coli, et al., 2011), b) (Afifpour, et al., 2014)

A bimrock is defined here as: a mixture of rocks, composed of geotechnically significant blocks within a bonded matrix of finer texture (Medley, 1994).

Geotechnical significance means (Medley, 1999):

- blocks must be stronger than the matrix, and the suggested minimum strength contrast between blocks and matrix is:

$$\tan \varphi_{block} / \tan \varphi_{matrix} \geq 2.0 \text{ (Medley, 2001).}$$

- The sizes of the blocks in bimrocks can vary widely, ranging from 5% to 75% of the size of the object being studied. For example, in a tunnel, the blocks might be 5% to 75% of the tunnel's diameter.
- The amount of volume taken up by the blocks in a bimrock can vary from very low percentages up to 75%.

1.2. Bimrock identification challenges

Bimrocks can be difficult to identify due to several factors:

- **Visual Similarity:** The blocks and matrix in a bimrock often have similar colors, textures, and mineral compositions, making it difficult to distinguish them visually.
- **Scale Dependence:** Identification can vary with scale; what appears as a block at a large scale might resemble a grain at a smaller scale.
- **Degree of Fragmentation:** Weathering and deformation can fragment or round the blocks, blurring the distinction between blocks and matrix.
- **Lack of Standardized Definitions:** The absence of a universally accepted definition for bimrocks results in inconsistencies in classification and identification.

To address these challenges, typically a combination of field observations, laboratory techniques (e.g., thin section analysis, X-ray diffraction), and geophysical methods like seismic surveys are used for an accurate identification of bimrocks.

Figure 1-4 shows the different layers of rock and soil in a bimrock formation. The information is based on data collected from drilling a borehole (Medley, 1999).

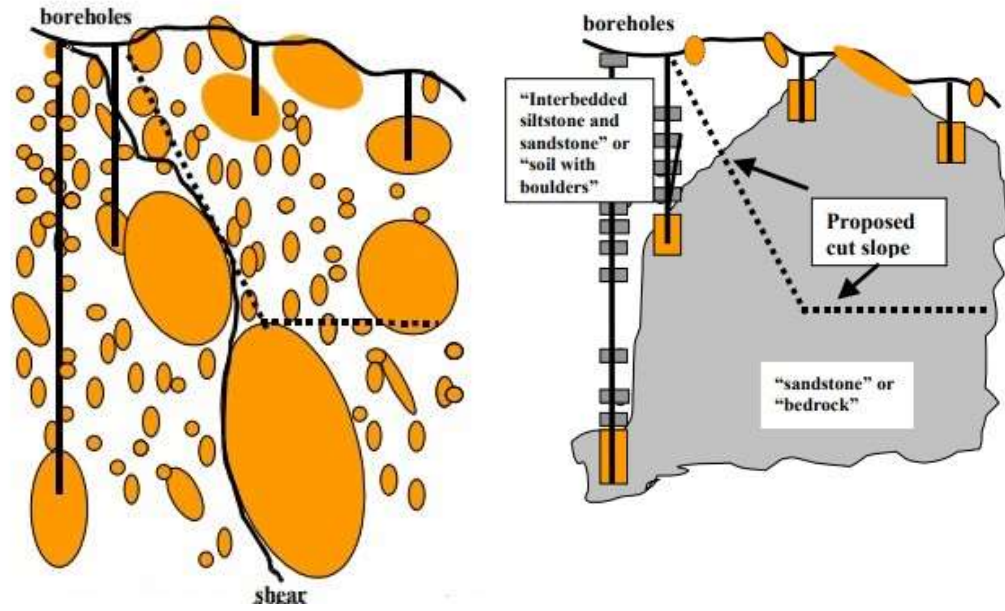


Figure 1-4 Rock Mass in Bimrock formation (The dashed line on the map shows the planned area for the road cut) (Medley, 1999)

1.3. Bimrocks Characteristics

Different studies on various types of bimrocks have shown that they share certain common features. These features are discussed in what follows.

1.3.1. Block size distribution

Studies have shown that the sizes of the blocks in bimrocks follow a pattern that is often seen in nature, called a fractal pattern ((Medley, 1994), (Medley, 2001)). They are defined by the negative power law given as follows (Turcotte, 1986):

$$N = n^{-D} \quad 1-1$$

Here, N denotes the relative frequency of elements within a specific frequency class n. The exponent D is referred to as the "fractal dimension" (Turcotte, 1986). The fractal dimension D is defined by (Peitgen, et al., 1992) as:

$$D = \frac{\log N(n)}{\log(n)} \quad 1-2$$

In theory, the power law implies that smaller blocks in a heterogeneous material occur more frequently than larger ones. The block size distribution influences the bimrock strength. (Lindquist, 1994) indicated that failure surfaces in a physical model of mélange bypassed the blocks, and the increase in the frictional component of strength (ϕ) was attributed to the tortuosity of the failure surfaces as they navigated around the blocks.

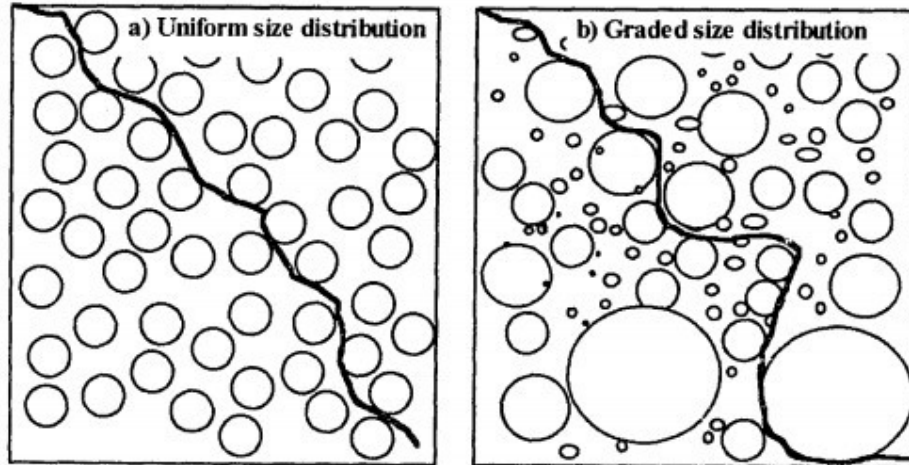


Figure 1-5 The impact of block size distribution on the "roughness" of failure surfaces was examined for two different distributions having the same block volumetric proportion (Lindquist, 1994).

Figure 1-5 illustrates the effect of varying block size distribution on the apparent roughness of the failure surface for two block configurations with approximately the same block volumetric proportion. The graded distribution results in a more tortuous failure path, even though the blocks are unrealistically smooth and rounded.

1.3.2. The Concepts of Self Similarity and Fractal

Dimension

The disorder found in mélanges, as illustrated in Figure 1-6, can be systematically analyzed using the concept of self-similarity, a component of the broader field of fractal studies.

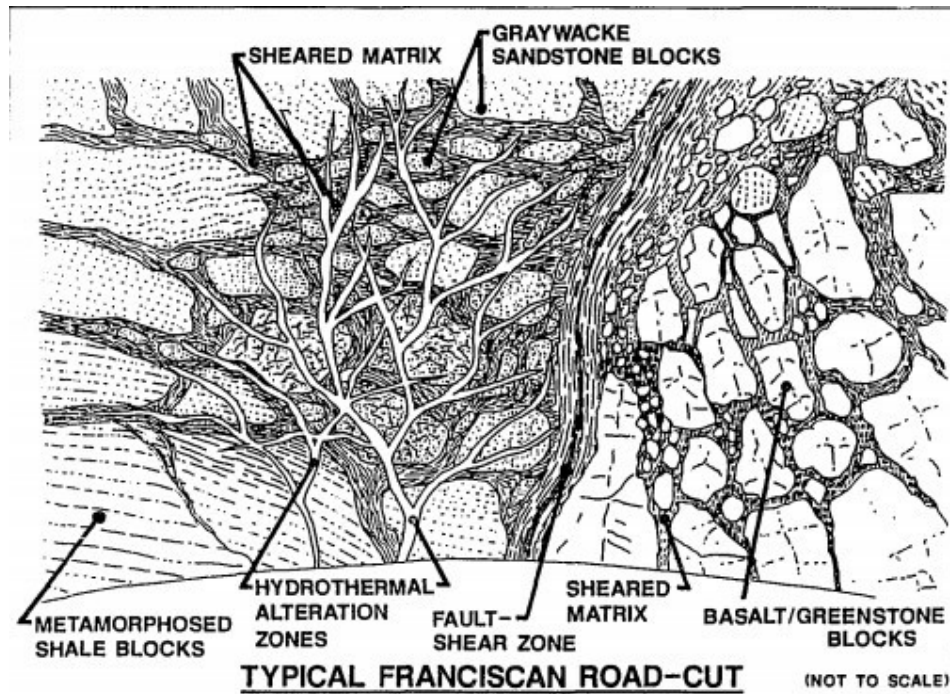


Figure 1-6 The disorder of Franciscan melange exposed at a road cut (Medley, 1994).

Research by (Cowan, 1985) showed that images of mélanges appeared similar when viewed at different scales. (Lindquist, 1991) later adopted a more quantitative approach to this issue, followed by additional studies conducted by (Medley, et al., 1995).

(Medley, 1994) continued the research done by Lindquist and examined over 1900 blocks in different Franciscan melanges. He found that the sizes of these blocks followed a pattern that was consistent at different scales and measured the largest size of the blocks in different photographs and maps of various scales. The maximum observable dimension of an outcropping rock block (d_{mod}) is shown in Figure 1-7.

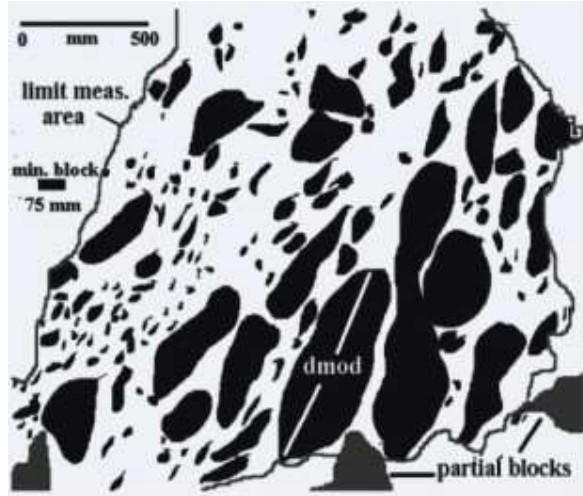


Figure 1-7 Franciscan mélangé outcrop at Caspar Headlands, Mendocino County, Northern California, displaying the dmod: maximum observed dimension (Medley, et al., 1995).

(Medley, 1994) created histograms that showed the frequency of different block sizes in Franciscan melanges. He divided the blocks into different size classes and calculated the size of each class using a specific formula. Two of these histograms are shown in Figure 1-8. The histograms consist of three sections: an ascending segment from left to right, followed by a peak, and then a descending segment. Despite significant differences in block size and the area studied, these log histograms appear similar.

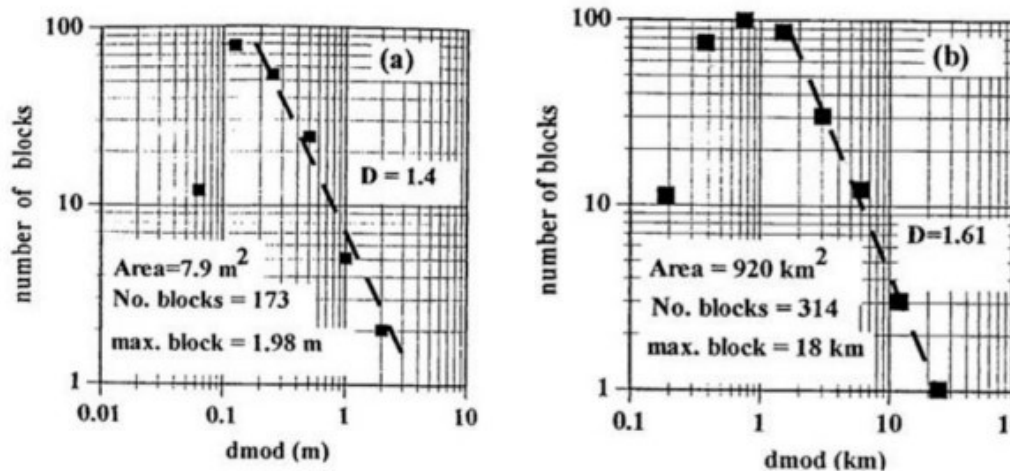


Figure 1-8 Log-log histograms for two distinct areas (Medley, 1994).

(Medley, 1994) compared numerous histograms by normalizing them as follows:

- The number of blocks in each size group was divided by the total number of blocks to get a percentage. This made the data independent of the size of the area being studied.
- The maximum observable dimension (d_{mod}) was converted to a unitless value by dividing it by \sqrt{A} , where 'A' is the area of the studied sites.

Following this procedure, numerous log histograms from various areas were created and illustrated in Figure 1-9. The peaks of all curves are approximately located at $0.05\sqrt{A}$, with a lower relative frequency to the left of the peaks because the blocks become too small to measure accurately. The largest block size is \sqrt{A} for any relevant scale, and since 99% of the blocks are smaller than $0.75\sqrt{A}$, this value is defined as the maximum block size (d_{max}). Moreover, blocks up to $0.75\sqrt{A}$ play a significant role in the volumetric block proportion.

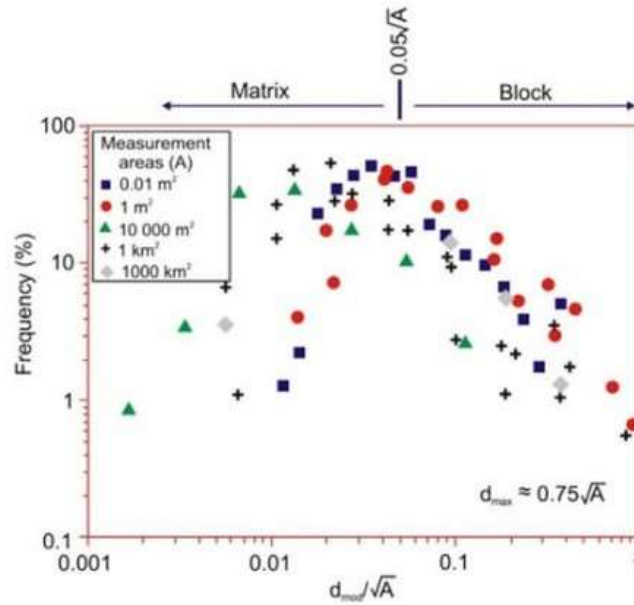


Figure 1-9 Compilation of log-histograms for the block sizes of 1,900 blocks in Franciscan mélanges, with sizes ranging from millimeters to kilometers (Medley, 1994).

1.3.3. Block-matrix threshold

(Medley, et al., 1995) determined that the size of the smallest block in a mélange should be 5% the characteristic engineering dimension (L_c , or \sqrt{A}). This means that blocks smaller than $0.05L_c$ are considered part of the matrix. This is because very small material has a minimal impact on the strength and other properties of bimrocks. The largest block is usually considered to be about $0.75L_c$. There are different ways to express this relationship, using L_c , the area (A), or the size of the largest block (d_{max}). For example, the threshold between matrix and blocks can be expressed as $0.05L_c$, $0.05\sqrt{A}$, or $0.05d_{max}$. (Medley, 2001) studied a 100 square meter area of Franciscan Mélange and determined that the characteristic engineering length was 100 meters. Based on this, blocks smaller than 5 meters would be considered part of the matrix, and blocks larger than 75 meters would be considered the largest possible blocks.

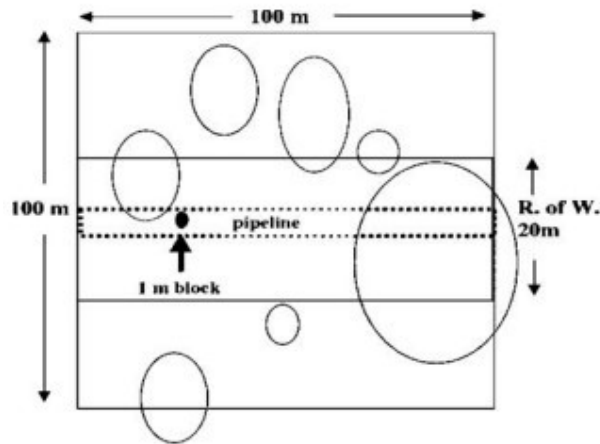


Figure 1-10 sketch illustrating different scales of interest for an area and the concept of block/matrix threshold, with the right side labeled "Road Width 20m." (Medley, 2001).

Based on Figure 1-10, if we are building a road, the characteristic engineering length (L_c) would be 20 meters, which is the width of the road. In this case, blocks that are 1 meter or larger would be considered significant and could cause problems during construction. Blocks smaller than 1 meter would be considered part of the matrix.

1.3.4. Volumetric Block Proportion (VBP)

Volumetric Block Proportion (VBP) is a term used to quantify the relative abundance of blocks within the matrix. It's calculated as the ratio of the total volume of blocks to the total volume of the bimrock mass. A higher VBP indicates a greater concentration of blocks within the matrix, while a lower VBP suggests a more matrix-dominated material.

1.3.4.1. Estimating VBP

Estimating VBP in bimrocks can be challenging due to the heterogeneous nature of these materials. However, several methods can be employed:

One-Dimensional (1D) Methods:

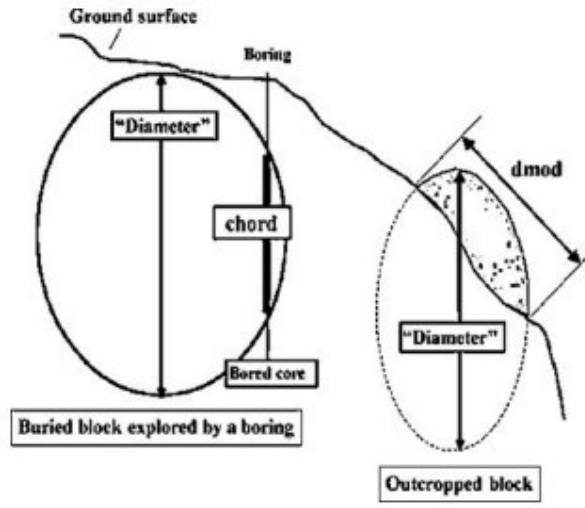
- Linear Block Proportions (LBPs): in 1D drilling explorations, LBPs are used to estimate VBPs. These involve measuring block proportions along scan lines on slabs cut from cubic physical models. The Monte Carlo-type approach is then applied to analyze uncertainties between assumed LBPs and true VBPs (Najafvand, et al., 2024).
- Drill Core/Block Intersection Lengths (Chords): by measuring the lengths where drill cores intersect blocks, 1D estimates can be obtained (Kahraman, et al., 2014). Collecting rock cores and visually estimating the block volume and matrix volume can provide a direct measurement of VBP (Figure 1-11a).

Two-Dimensional (2D) Methods:

- Geological Mapping: mapping and image analysis on scanned images or photographs provides 2D estimates of VBPs (Tien, et al., 2010). Using digital images of rock samples and image processing techniques to quantify block and matrix areas can estimate VBP (Figure 1-11b).

Three-Dimensional (3D) Methods:

- Sieve Analyses: these provide 3D estimates of VBPs.
- Virtual Drilling Programs: This approach was used to identify a chart that assists in determining a correction factor necessary for deriving a range of VBP from in-situ measurements. (Napoli, et al., 2022).



a



b

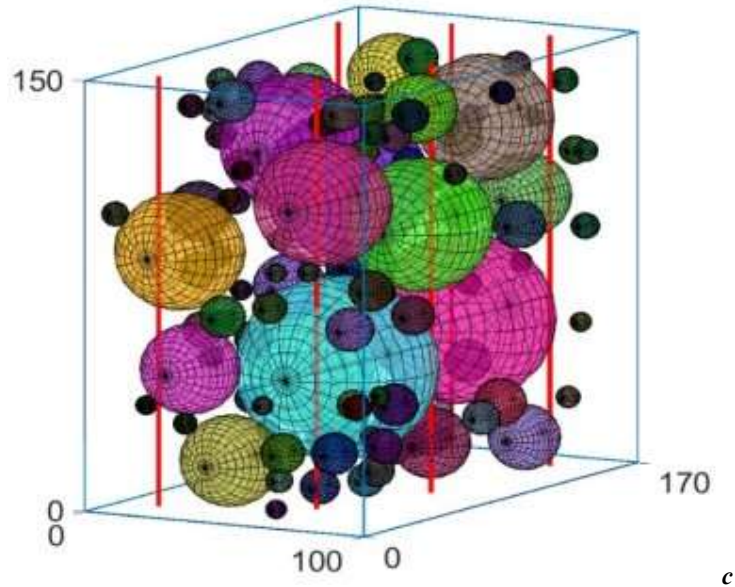


Figure 1-11 (a) Core Analysis (Medley, 2001), (b) Image analysis (Lindquist, et al., 1994), 32%VBP virtual bimrock model with example virtual borings (dimensions in millimeters) (Napoli, et al., 2022).

Numerous factors influence how successful the one-dimensional technique is. First, how the blocks are oriented in relation to the direction of drilling. It refers to whether the block is encountered at its diameter or chord while drilling, as seen in Figure 1-11a. Drilling in chord length causes a phenomenon known as "tailing," which frequently causes the block size to be underestimated. The volumetric block proportion is also an important factor affecting the estimation of the VBP. Higher VBP increases the likelihood of running into a block during drilling, which reduces uncertainty. Lastly, the efficacy of the one-dimensional approach for VBP estimate is also influenced by the entire length of drilling. At least ten times the greatest block size should be used as the drilling length, according to (Medely, 1997), (Napoli, et al., 2022).

The 1D (chord) distribution and the 3D block size distribution were examined by (Medley, 2001). It was discovered that the 3D block size distribution is not perfectly replicated by the 1D distribution. The 1D chord distribution overestimates the tiny size blocks as a result of tailing. A comparison is displayed in Figure 1-12.

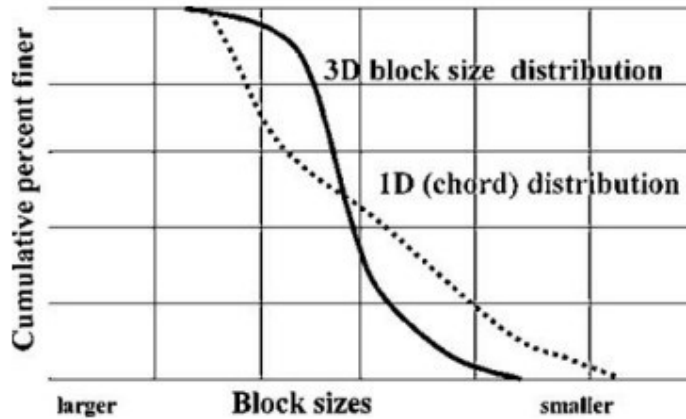


Figure 1-12 The 3D block size distribution is only marginally replicated by the 1D chord distribution. 1D chord overestimates the smaller diameters and underestimates the bigger block size (Medley, 2001).

In order to describe the estimation of the volume percentage of the blocks in the considered domain based on the assumption that they are the same as the measured linear block proportions, (Medley, 2001) established an experimental approach by drawing scanlines on the specimen side or image analysis of their exteriors. He created physical mélange models using hundreds of model boreholes and known block size distributions and volumetric block proportions. The results of the studies indicated that in order to get a suitable estimate of the volumetric block proportion, measured linear block proportions needed to be corrected by an uncertainty factor.

Although these measurements are often not the same as volumetric proportions, (Medley, 1994), (Napoli, et al., 2022), (Napoli, et al., 2021) presented techniques for estimating block proportions using scanlines drawn on the side of specimens or image analysis of specimen exteriors.

A plot between $N * d_{max}$ and SD/Vv , which is regarded as a measure of uncertainty, was created in order to ascertain the uncertainty, as seen in Figure 1-13. In this case, Vv is the actual volumetric proportion and SD is the standard deviation of the linear proportion.

The curve in Figure 1-13 shows that when the volumetric percentage rises, with an increase in sample duration, uncertainty likewise reduces.

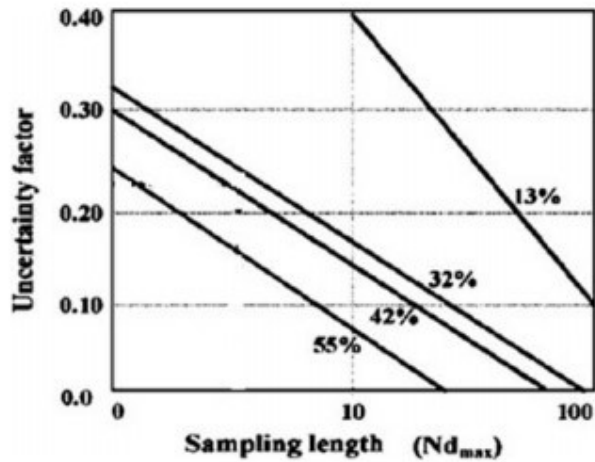


Figure 1-13 Uncertainty in the estimated values of VBP in relation to the measured linear block proportion (13 to 55%) and the length of linear measurement (LBP), which is expressed as a multiple (N) of the length of the biggest block (d_{max}) (Medley, 1997).

In order to compare these data with the 3D Block Size distribution (3D BSD), (Medley, 2001) went over it again. The comparison between the 1D Chord Length Distributions (1D CLDs) and the 3D BSD reveals very little agreement. Figure 1-14 displays the comparison's outcome. The impact of boring-induced "tailing" is explained. Compared to the actual 3D BSD, more smaller-sized blocks were produced.

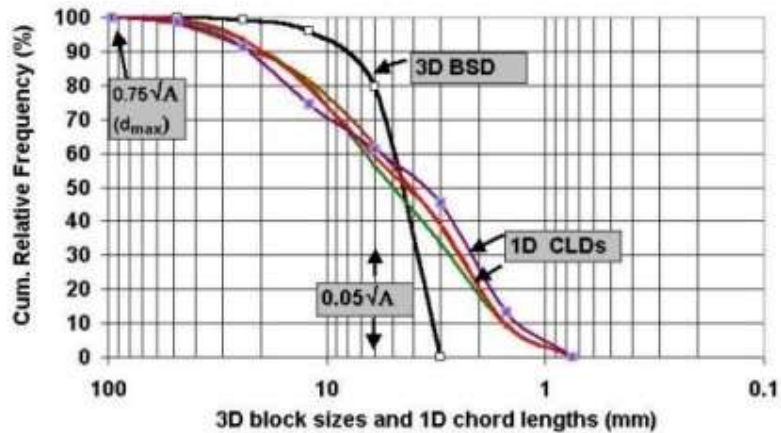


Figure 1-14 A comparison of the 1D chord length distributions and the 3D block size distributions
(3D BSD and 3D CLD) (Medley, 2001).

1.4. Mechanical characteristics of Bimrocks

Mechanical characterization of Bimrocks presents several unique challenges due to their heterogeneous and anisotropic nature. Here are some of the main challenges:

(Lindquist, 1994) found that the total strength and deformation qualities of the material are directly correlated with the VBP in a physical model mélange.

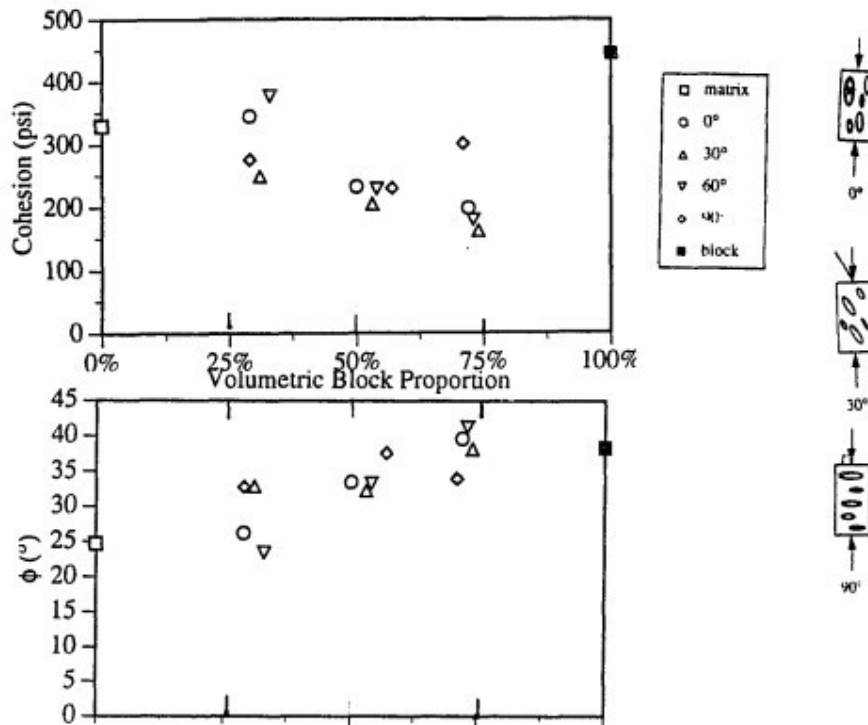


Figure 1-15 The influence of block volumetric proportion on the cohesion and friction angle of physical model mélanges was assessed through triaxial compression tests on 150 mm diameter specimens (Lindquist, 1994).

As the block percentage climbed over a lower threshold proportion of 25 percent, as Figure 1-15 illustrates, cohesion reduced, the friction angle ϕ increased, and the modulus of deformation increased. (Lindquist, 1994) also reviewed three distinct research, he observed that there is a trend toward a higher friction angle and an increase in VBP which is depicted in Figure 1-16.

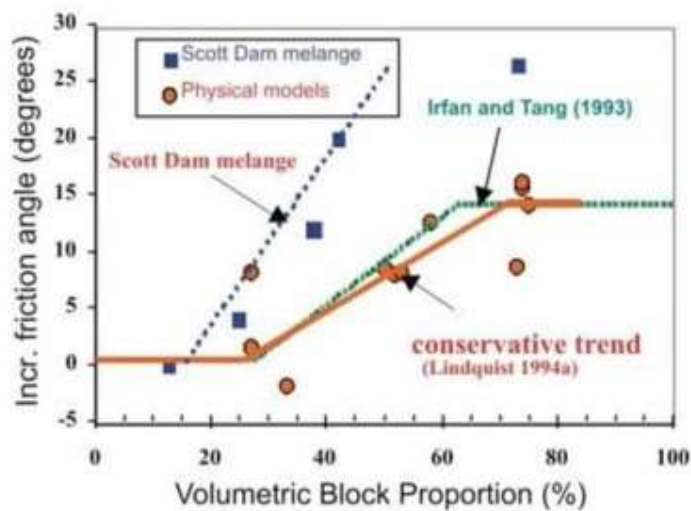


Figure 1-16 rising trend in the friction angle in different investigations studies (Lindquist, 1994).

Several investigations that have been performed to ascertain the mechanical properties of bimrocks are listed below.

- **Laboratory Tests**

Bimrocks are substantial heterogeneous materials, as was previously proven. Bimrocks are therefore challenging to investigate on a small scale. Therefore, to replicate the characteristics of bimrocks., researchers created lab-scale imitations. In such experiments, samples were created comprising a certain block content and a weaker matrix. These illustrations were then put through a laboratory test. The impact of block orientation and content on bimrocks' mechanical characteristics were

examined. In the written word, a few of these studies consist of investigations into the influence of block content and orientation on the mechanical properties of bimrocks ((Afifipour, et al., 2014), (Hu, et al., 2024), (Lindquist, 1994), (Kalender, et al., 2014)).

In the laboratory, (Lindquist, 1994) performed a series of triaxial compression experiments on the artificially created physical bimrock samples. The samples were composed of a bentonite-Portland matrix and elliptical-shaped blocks comprised of a sand-Portland cement-fly ash combination. The major to minor axis ratio of the blocks was 2:1. The samples had diverse block compositions varying between 25% to 75%.

The impact of the block inclusions' orientation with respect to the vertical direction of the load application on the mechanical characteristics of bimrocks was also examined by the author. Four different block orientations were studied: 0°, 30°, 60°, and 90°. The four distinct rock block orientation angles in relation to applied load are displayed in Fig. 1.17.

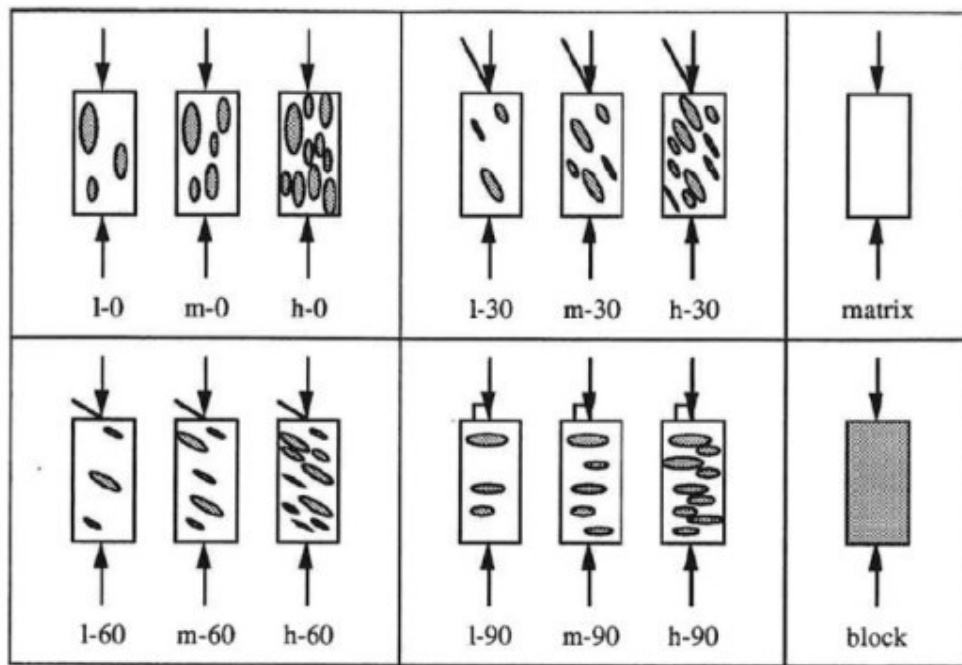


Figure 1-17 manufactured specimens of bimrocks by four different block orientations .

(Lindquist, 1994).

According to test results, bimrocks' friction angle increased to between 15 and 20 degrees, while their VBP increased to between 25 and 75 percent. Conversely, cohesion exhibited a declining tendency as VBP increased.

Due to the fact that blocks are stiffer than the matrix, it was discovered that the failure plane entered the block-matrix contacts. The poor mechanical qualities of the matrix in the interface along the block edges, where deformations tend to occur, are the cause of the drop in cohesion. Hence, a higher block fraction corresponds to a greater number of dispersed weak regions and lower cohesion. The tortuosity of the failure surface causes an increase in the friction angle. This happens because the blocks and matrix have a strong mechanical contrast, meaning that the blocks have a greater geotechnical significance.

(Hu, et al., 2024) investigates the influence of rock block proportion on the mechanical properties of Bimrocks under different block-to-matrix strength ratios using a new indoor test method. Strength and failure characteristics of samples with varying VBPs under varying matrix-block strength ratios are examined using the indoor uniaxial compression Strength (UCS) test and the direct shear test.

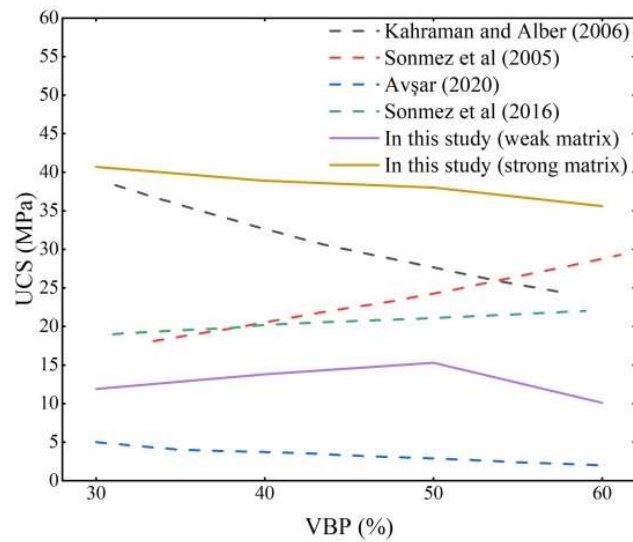


Figure 1-18 Comparing VBP and UCS changes in present and previous studies (Hu, et al., 2024).

Figure 1-18 depicts that the UCS of the strong matrix samples gradually declines as VBP rises, while the UCS of the weak matrix samples generally exhibits a rising

tendency. However, when the VBP is bigger than 60%, the strength is decreased (Hu, et al., 2024).

(Yazdani, et al., 2024) investigated the influence of rounded blocks on the shear characteristics of hard-matrix bimrocks, which are similar to various conglomerates. A sequence of laboratory direct shear tests was conducted on idealized models composed of glass bead blocks bonded by matrix plaster, with different volumetric block proportions (VBP). Figure 1-19 depicts the stages involved in sampling.

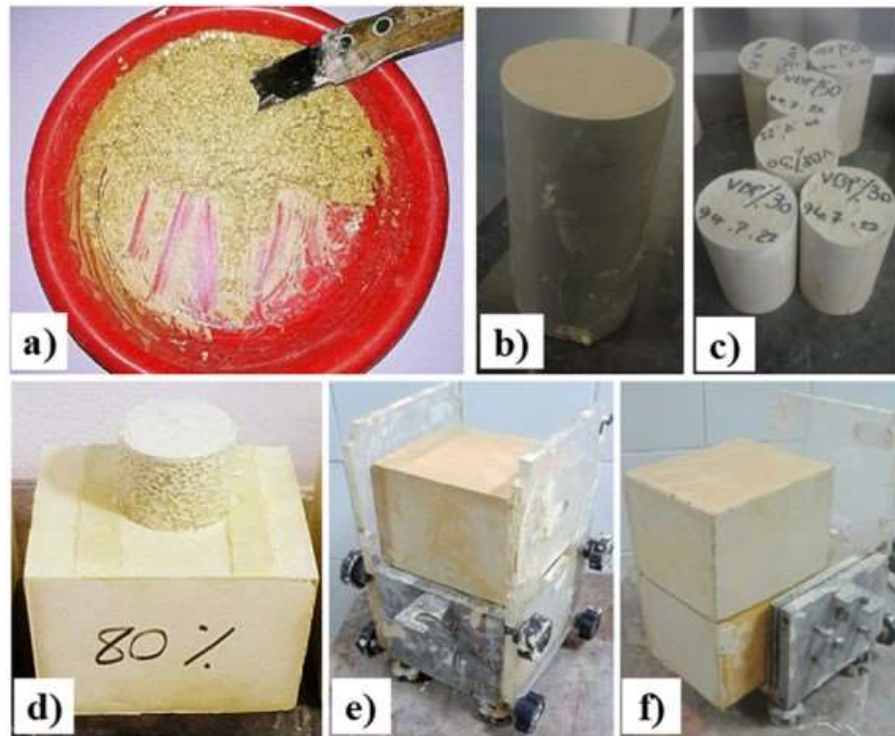


Figure 1-19 the stages involved in sampling: (a) a synthetic block-in-matrix mixture prior to being poured into the mold, (b) a standard molded mixture, (c) six representative cylindrical bimrock samples, (d) a cylindrical sample following the molding of the initial half, (e) the process of molding the second half, and (f) the removal of the completed sample from the mold (Yazdani, et al., 2024).

The calculation of the breakage factor (BF) can be determined by assessing the ratio of the number of failed blocks (FC) to the overall total of blocks (BC) present

within the shear zone. (Yazdani, et al., 2024) found that block breakage factor (BF) occurred most commonly in samples that were situated within the suggested VBP range for typical bimrocks (specifically, 25%–75%), with particular emphasis on samples exhibiting VBPs of 40%, 50%, and 60%. Additionally, Figure 1-20 illustrates that as VBP rises within this recommended range, block failure initially escalates, peaking at a VBP of 50% before experiencing a decline. This upward trend is associated with an increased frequency of block-to-block interactions within the shear zone, which subsequently raises the probability of block collisions during shear.

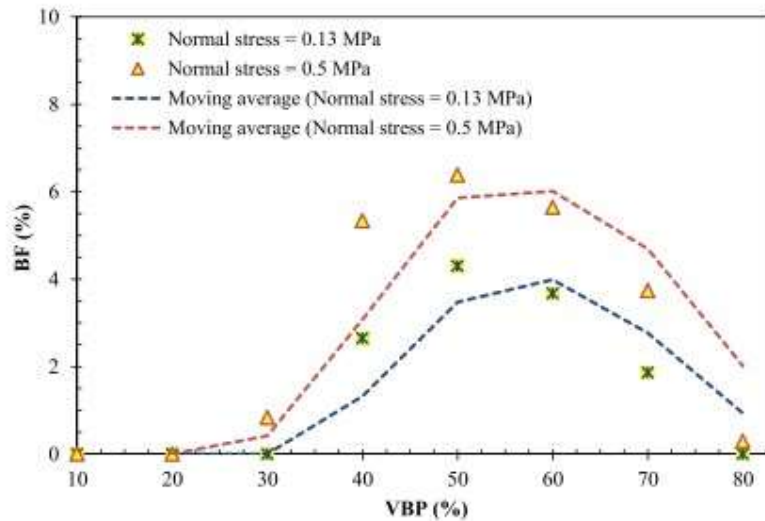


Figure 1-20 Correlation between BF and VBP (Yazdani, et al., 2024).

- **In-Situ Tests**

Large-scale testing was conducted at the Italian Santa Barbara open-pit mine. The Santa Barbara mining area is home to several Shale-Limestone Chaotic Complex (SLCC) bimrocks. Six unconventional shear tests were conducted by (Coli, et al., 2011) and dubbed "BimTests." These tests were called non-conventional in contrast to shear testing that is standardized.

The Mohr-Coulomb parameters, c and ϕ , were determined by the use of the simplified limit equilibrium criteria. The trend, which demonstrated a declining trend

in cohesiveness and a rise in friction angle with an increase in VBP, supported the findings of past research.

(Zhang, et al., 2016) conducted a comparable large-scale direct shear test in-situ. They evaluated the influence of rock block inclusions in soil utilized for the core wall of a high embankment dam in China. They carried out four direct shear tests under varied normal loads and compared the results with that of pure soil.

35% of the sample consisted of blocks. A hardening phase before the peak strength was observed by the stress-strain SRM' curve. In general, the peak strength was greater than that of the matrix-only. There was a 7° rise in the friction angle and a 35 kPa drop in cohesion. Figure 1-21 illustrates the connection between shear strength and normal stress. In the plot, SRM stands for "Soil Rock Mixture," a more often used alternative word for bimrocks or bimsoils among Chinese academics.

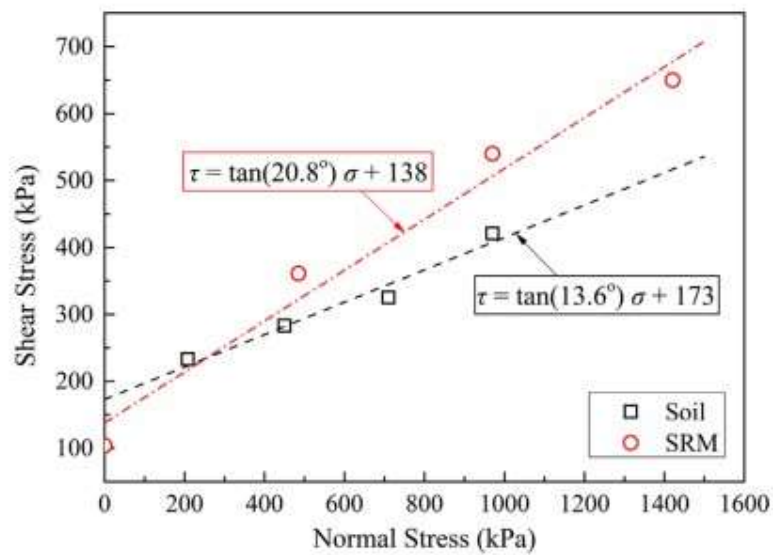
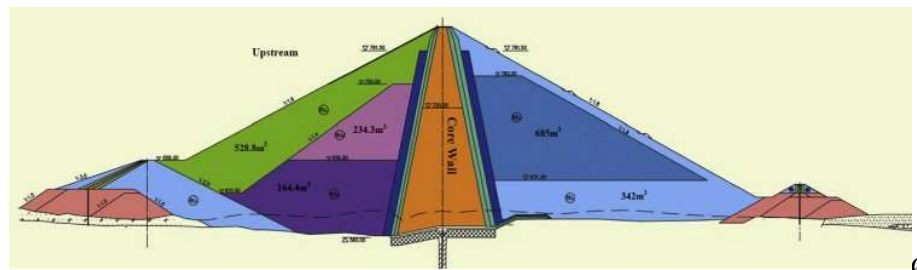


Figure 1-21 (a) Main section of the Nuozhandu embankment dam, (b) The relationship between shear strength and normal stress of the test samples (Zhang, et al., 2016).

- **Numerical Methods**

For the intricate mechanical behavior of bimrocks, numerical approaches are essential. Traditional analytical approaches are insufficient for bimrocks because of their diverse composition, which results in distinctive reactions including non-linear deformation and varied failure patterns. The Finite Element Method (FEM), Finite Difference Method (FDM), and Discrete Element Method (DEM) are the main numerical techniques for bimrock analysis.

The rock mass is divided into a mesh of elements (triangles, tetrahedra, etc.) via the Finite Element Method (FEM), which then solves equations regulating the material behavior at each element. Its primary benefit is that it can handle intricate geometries and material characteristics, which makes it appropriate for modeling bimrock failure, deformation, and stress-strain response.

In contrast, the Finite Difference Method (FDM) approximates derivatives using finite differences at discrete locations on a grid. It is frequently used to simulate heat transfer, fluid movement, and wave propagation in bimrocks and is easier to construct for regular geometries.

On the other hand, the Discrete Element Method (DEM) captures the discontinuous behavior of bimrocks by modeling the rock mass as a collection of discrete particles (blocks and matrix grains) that interact through contact forces. DEM is ideal for simulating rock fragmentation, slope stability, and tunnel excavation in bimrocks, however several unknown parameters have to be set.

(Barbero, et al., 2008) investigated the mechanical behavior of bimrocks, a heterogeneous material with strong blocks in a weaker matrix, which poses engineering challenges. Using 3D Finite Element Method simulations, the study analyzes uniaxial and triaxial compression tests for different block volumetric proportions. Results show that block volume and block-matrix interfaces significantly impact bimrock's strength and deformability, confirming the trends observed in earlier 2D studies.

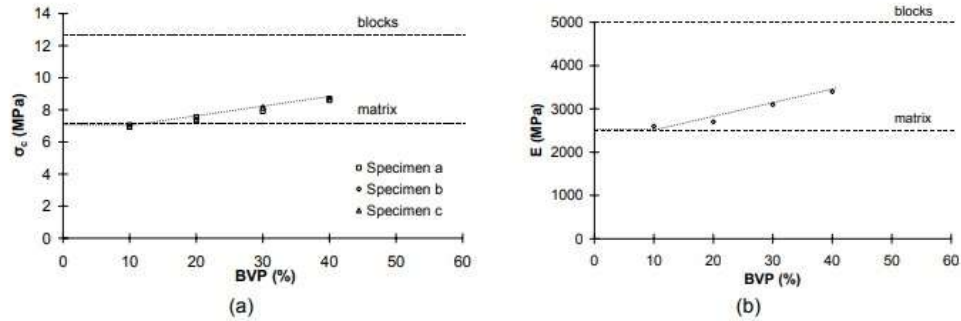
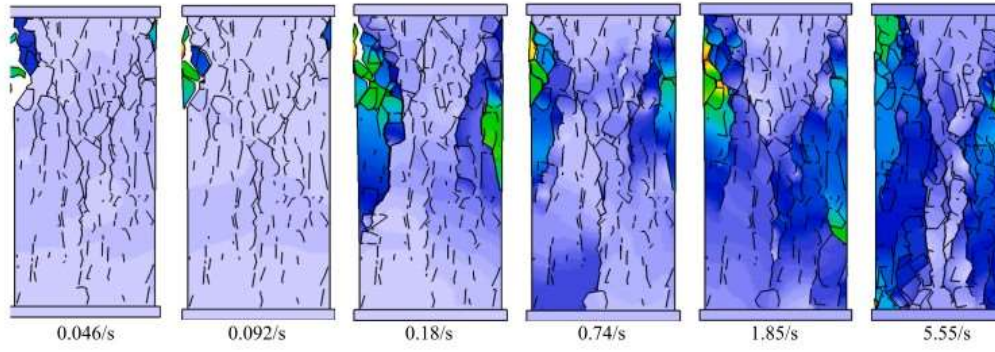


Figure 1-22 Impact of the (VBP) on bimrock specimens' (a) unconfined compressive strength and (b) average deformation modulus (Barbero, et al., 2008).

As illustrated in Figure 1-22 while block arrangement can influence localized yielded zones, bimrock's mechanical reaction at low VBP, like 10%, is uniformly yielding and matches that of the matrix alone. At VBP = 20%, a threshold is reached, after which the blocks start to have a noticeable effect. The bimrock's tangent deformation modulus and compressive strength both exhibit a linear rise with increasing VBP up 40%, after which data are not available. This suggests that greater VBP values improve bimrock's strength and stiffness.

(Sharafisafa, et al., 2024) evaluated the impact of strain rate on the failure and stress-displacement behavior of bimrock with different volumetric block proportions VBP, ranging from 50% to 90%, using the combined finite-discrete element technique (FDEM). Based on earlier research, six strain rates 0.046/s, 0.092/s, 0.18/s, 0.74/s, 1.85/s, 5.55/s were chosen. The results showed as the VBP escalates, the strain rate becomes increasingly significant and pronounced. The most vulnerable areas within a bimrock are located at the interfaces between blocks and the matrix. An elevated VBP suggests a greater number of these interfaces subjected to loading and heightened stress concentration. Consequently, this leads to a rise in interface failure, resulting in more complex fracture planes. Additionally, the influence of tensile failure intensifies with the increasing strain rate. Figure 1-23 shows failure of VBP 75% under different strain rates.



***Figure 1-23 Failure of the bimrock specimens with VBP of 75% under various strain rates
(Sharafisafa, et al., 2024).***

2. Tunneling

2. Benefits from tunneling

A tunnel is a confined corridor that traverses or is situated beneath an obstruction, facilitating a pathway for multiple uses. Tunneling offers several benefits, including minimal surface disruption, which preserves land for other uses and reduces noise pollution and ecological impact. It enhances transportation efficiency by reducing traffic congestion, connecting isolated areas, and providing safer routes through challenging terrains. Additionally, tunnels help maintain the aesthetic integrity of landscapes and protect heritage sites or residential areas from disturbances. By keeping infrastructure underground, they create a more sustainable and less intrusive solution for urban development and transportation needs.

2.1. Tunnel construction techniques

Tunnel construction techniques vary depending on factors such as the geological conditions, tunnel length, diameter, and intended use. Here are some common methods:

2.1.1. Conventional Methods

Tunnel construction techniques encompass various approaches, including Drill and Blast for challenging rock formations, Cut and Cover for shallow tunnels in urban environments, Shield Tunneling for softer ground conditions, and Pipe Jacking for tunnels with smaller diameters. Each technique is characterized by distinct applications and factors to consider, such as the generation of noise and vibrations associated with Drill and Blast, as well as the appropriateness of each method for varying geological conditions.

2.1.2. Full face mechanized Methods and improvement's techniques

- **Tunnel Boring Machines (TBMs):** TBMs are big, mechanized devices that remove excavated material from the earth by cutting through it. They work well in a range of geological settings and are quite efficient. They suggested how to choose and

size TBMs, what geological circumstances might restrict their use, and how crucial it is to conduct in-depth geological and geotechnical studies in order to comprehend the conditions of the rock mass.

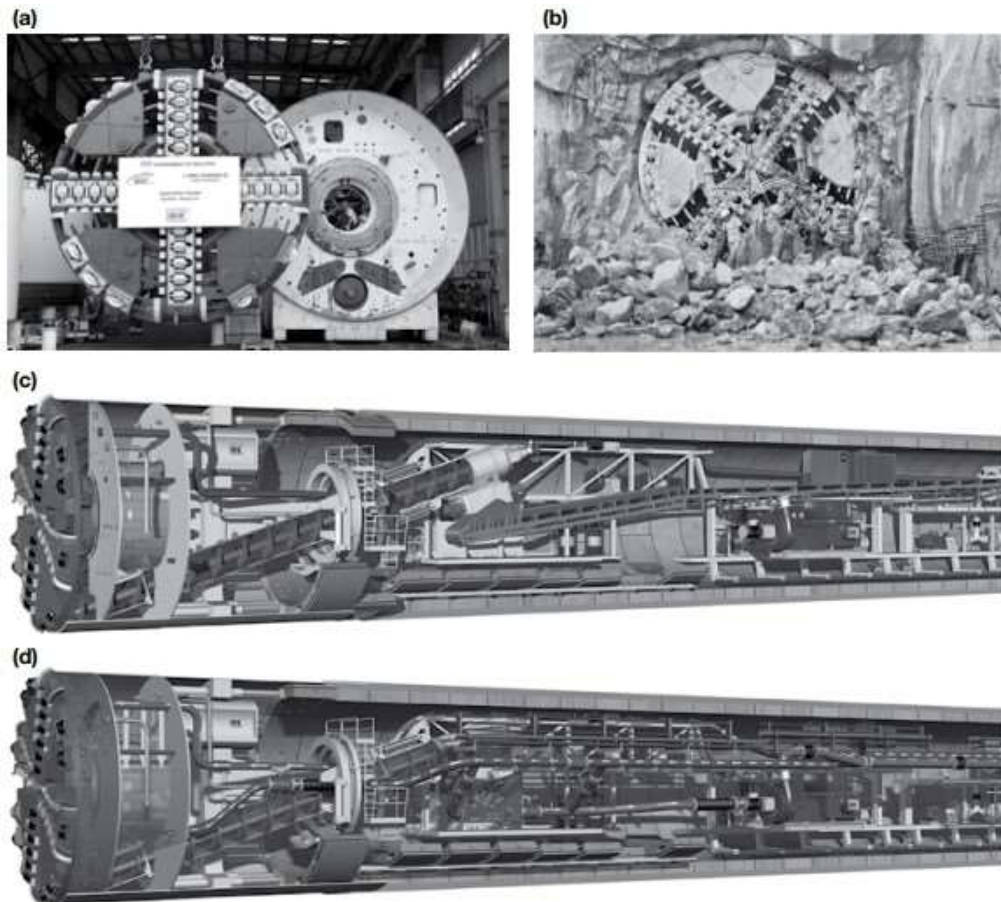


Figure 2-1 The Klang Valley multimode tunnel boring machine (TBM) features a diameter of 6.62 meters. (a) the TBM cutterhead is depicted within the factory, the excavation chamber (plenum) and the terminal section of the screw conveyor. (b) the TBM is illustrated upon the completion of a drive, highlighting the geological material it is penetrating. (c) the TBM is shown operating in Earth Balance Mode (EBM). (d) the TBM is represented in slurry mode, with visible connections for the slurry line. (Image credit: Herrenknecht.), (Chapman, et al., 2018).

2.2. Stability problems in tunneling

Tunnel stability is influenced by a multitude of factors associated with geological conditions, construction practices, and external environmental impacts. Geological challenges encompass issues such as squeezing and swelling of clay-rich soils, the presence of running ground characterized by loose sediments, instability in rock formations due to fractures or weak materials, and the ingress of water. Construction-related challenges stem from insufficient support systems, the use of unsuitable excavation techniques, and flawed sequencing of construction activities. Additionally, external influences, including seismic events, adjacent construction activities, and the gradual degradation of tunnel linings, further exacerbate stability concerns. Two prevalent techniques for ground improvement in tunneling, especially under soft ground conditions, are the freeze-thaw method and jet grouting. The freeze-thaw technique entails the process of freezing the soil or rock surrounding the intended tunnel excavation, thereby establishing a temporary, stable barrier of frozen material before the excavation commences. This approach offers essential support and mitigates the risk of collapse during the digging phase. Conversely, jet grouting involves the injection of high-pressure streams of water and cement (or alternative grout materials) into the ground, resulting in the formation of a reinforced soil mass that acts as a robust, in-situ wall prior to excavation. Both techniques are designed to enhance ground stability and reduce the likelihood of ground movement or collapse during tunneling operations in difficult soft ground conditions. (Barla, et al., 2000) investigated the difficulties of employing Tunnel Boring Machines (TBMs) in difficult geological conditions.

2.2.1. Deep tunnels

(Zhou, et al., 2014) evaluated the stability of the diversion tunnels of the Jinping II hydroelectric facility in China's Sichuan Province. The petrophysical characteristics, mechanical behaviors, and water-weakening qualities of chlorite schist were investigated in laboratory experiments. The study examined the ongoing distortion of the surrounding rock mass, the disintegration of support systems, and the large-scale

collapses brought on by high in situ stress and weak chlorite schist. Two reinforcing plans were proposed for the bottom segment of the tunnel's excavation based on these findings. Figure 2-2 shows one layout of the two tunnel bottom reinforcement schemes.

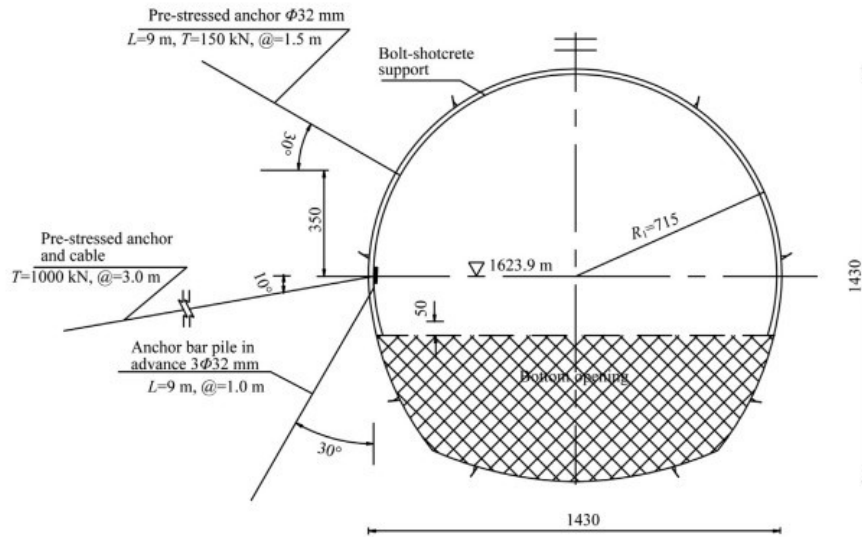


Figure 2-2 Layout of reinforcement scheme-1 of tunnel bottom (unit: mm), (Zhou, et al., 2014).

(Napoli, et al., 2021) researched the stability of a deep circular tunnel constructed within a heterogeneous rock mass characterized by a chaotic block-in-matrix structure. They assessed the influence of rock inclusions on the overall performance of the bimrock during the excavation process, employing various Volumetric Block Proportions (VBPs). To address the spatial and dimensional variability of the blocks, multiple heterogeneous tunnel configurations are created for each VBP through a stochastic methodology. They performed more than 40 2D numerical analyses by using the FEM code RS2. An illustration of the modeling process is provided by Figure 2-3.

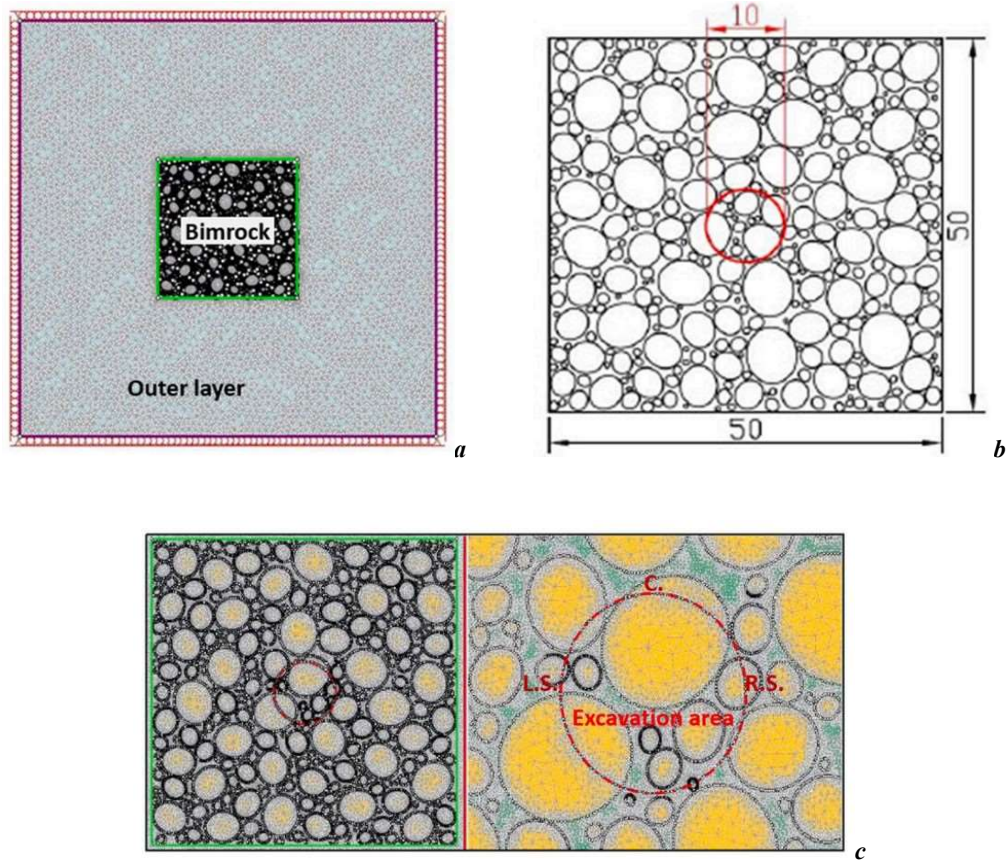


Figure 2-3 (a) Example of a modified rock mass in bimrock including a homogeneous outer layer, (b) An example of the final geometry, (c) A 70% VBP bimrock model with the tunnel indicated by a red circle is shown on the left. A close-up of the mesh created for the block-in-matrix area of the same bimrock model is shown on the right (Napoli, et al., 2021).

The simulations conducted on heterogeneous models indicate that the presence of blocks has a considerable impact on the behavior of bimrocks during underground excavation processes. The shear stresses, displacements, and formation of plastic zones are significantly influenced by both the presence and dimensions of blocks in proximity to the tunnel. The development of yielded zones occurs in a complex manner within the matrix, aligning with findings from earlier research. Analyses utilizing the Finite Element Method (FEM) demonstrate that even at a Volumetric Block Proportion (VBP) of 25%, blocks can lead to considerable fluctuations in the strength of the rock mass,

with these fluctuations becoming increasingly significant as VBP values rise (Napoli, et al., 2021).

2.2.2. Shallow tunnels

Shallow tunnels, owing to their close proximity to the ground surface, pose distinct stability challenges. One of the primary concerns is surface settlement, as any movement in the ground can adversely affect structures located above. Additionally, the reduced confinement and potential instability of both the tunnel face and crown, particularly when influenced by groundwater, present further complications. The construction process is further complicated by the necessity for specialized excavation techniques, strong support systems, and meticulous management of pre-existing utilities. Moreover, shallow tunneling can result in disturbances such as noise and vibrations, traffic interruptions, and various environmental issues. To address these challenges, effective mitigation strategies should encompass comprehensive ground investigations, suitable excavation and support methodologies, ground enhancement techniques, and diligent monitoring to reduce risks and minimize impacts on the surrounding environment and infrastructure.

In order to forecast and analyze ground motions brought on by shallow tunneling in soft ground, (Pinto, et al., 2013) present simpler analytical solutions. Compared to popular empirical approaches, these answers offer a more thorough knowledge of ground movement distribution. Assuming linear, elastic soil behavior, the research gives analytical solutions for ground displacement in two deformation modes: uniform convergence and ovalization at a circular tunnel wall. It demonstrates that, with the exception of extremely shallow tunnels, deformation fields generated from basic singularity solutions are comparable to those taking the physical dimensions of the tunnel into account. Furthermore, the research presents closed-form solutions for a 3D tunnel heading and presents a simpler approach to include soil plasticity in the analysis.

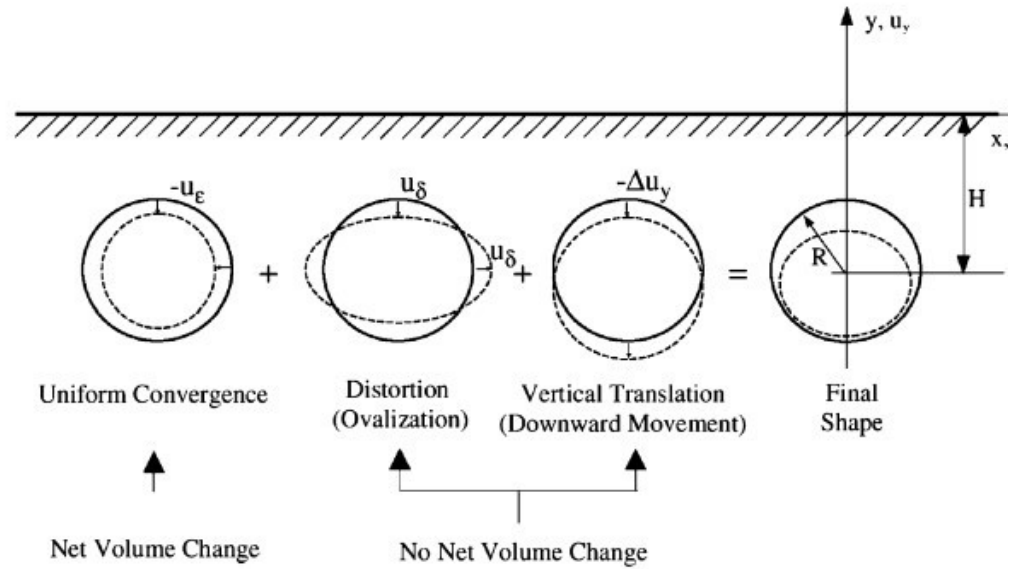


Figure 2-4 Modes of deformation and symbols for shallow tunnel (Pinto, et al., 2013)

(Patil, et al., 2018) By using the PLAXIS 2D AE.02 program, examined the effects of earthquake loadings on tunnels constructed on soft soil. In order to investigate different elements influencing the seismic response of the tunnel-soil system, they performed parametric studies. These variables include tunnel shape, input motion parameters, tunnel depth, lining thickness, and soil-tunnel interface conditions. According to the study, circular tunnels are better than other forms when subjected to seismic loading. More bending moment is experienced by square tunnels with rounded corners than by traditional square tunnels. Furthermore, the properties of the input motion have a major impact on the dynamic earth pressure on the tunnel lining. Figure 2-5 shows the schematic diagram of a two-dimensional numerical model.

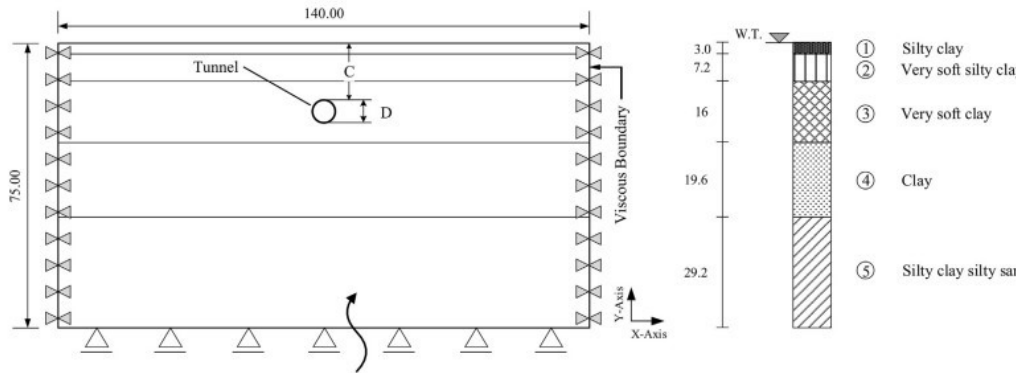


Figure 2-5 Schematic illustration of the numerical model (unit: m), (Patil, et al., 2018)

(R. Abdellah, et al., 2018) investigated the influence of two critical factors on the stability of shallow underground tunnels: the existence of rock joints within the rock mass matrix and the configuration of the excavation. The research employs a set of two-dimensional elasto-plastic finite-element models developed using RS2D software to evaluate these impacts.

The research indicates that the stability of tunnels deteriorates considerably following excavation, particularly in the case of square tunnels. This stability is further undermined by the existence of rock joints within the surrounding rock mass. The presence of these joints disrupts the continuity of strength contours around the tunnel's perimeter, resulting in heightened deformations and stresses at the boundary. Normal stress along the rock joints reaches its peak at the tunnel boundary but experiences a significant decline when the joints intersect the tunnel. At these intersections, the direction of shear stress reverses, leading to inward shear displacement. Nevertheless, despite these challenges, all tunnels are deemed satisfactory according to the established failure evaluation criteria, irrespective of the influence of rock joints or the shape of the tunnel.

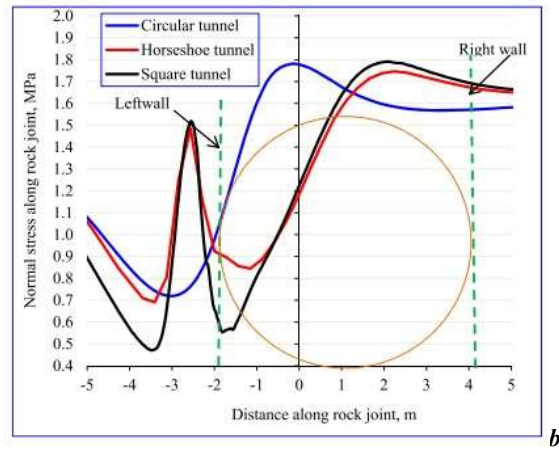
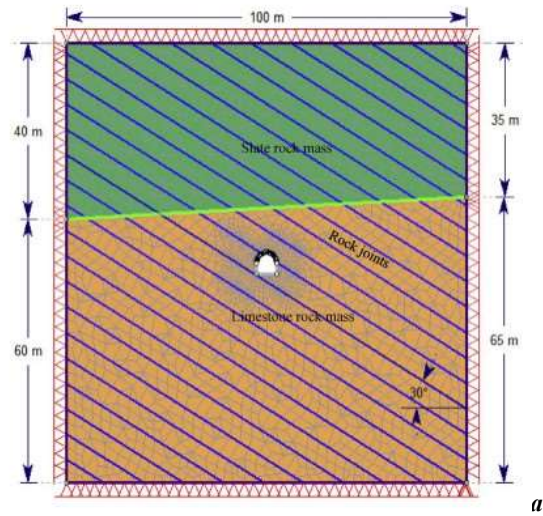


Figure 2-6 (a) Joint model, boundary conditions and the geometry of a horseshoe tunnel, (b) normal stresses along joints at distance ranges of ± 2.5 m from the centre of the tunnel , (R. Abdellah, et al., 2018)

(Shahin, et al., 2016) conducted a study on tunnel excavation in the context of an existing tunnel and a nearby building, employing non-linear finite element analyses through the FEMtij-2D software. Surface settlement in shallow and deep tunneling is shown in Figure 2-7.

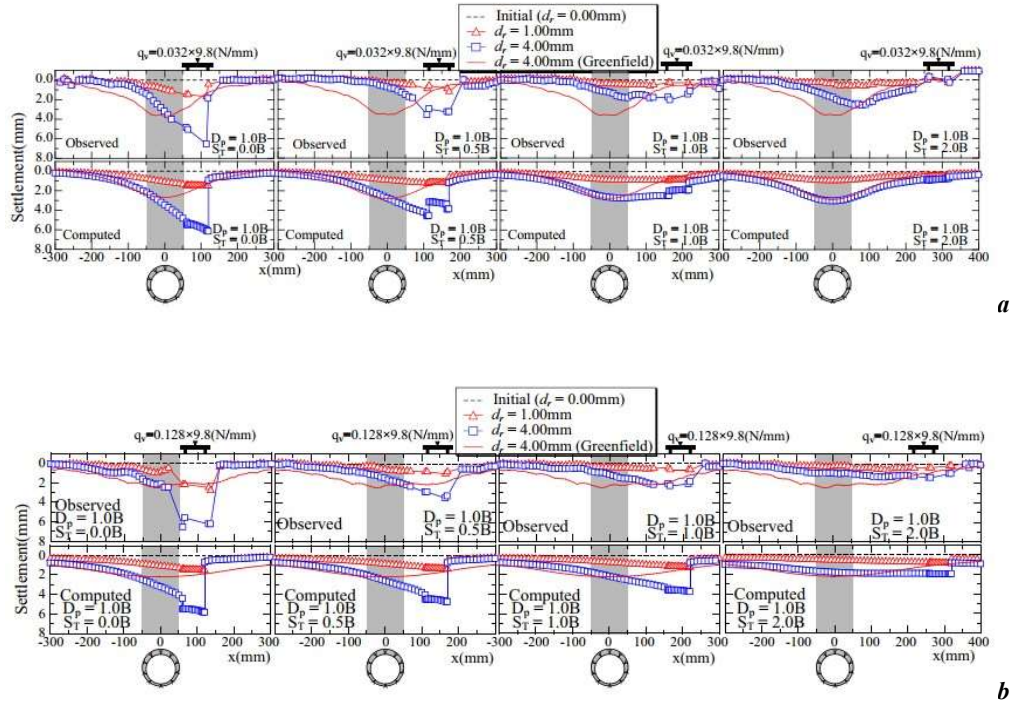


Figure 2-7 (a) Surface settlement in existing building loads: $D/B = 2.0$ (shallow tunneling), (b) Surface settlement in existing building loads: $D/B = 4.0$ (deep tunneling), (Shahin, et al., 2016).

The research indicates that the highest surface settlement during tunneling is observed at the location of the building load when the foundation is positioned at a specific distance. This suggests that the maximum settlement may not occur directly above the tunnel axis in the presence of adjacent superstructures. Within the tunneling influence zone, a shear band forms asymmetrically towards the tip of the pile. Furthermore, an uneven distribution of earth pressure is noted around the tunnel, contrasting with conditions in greenfield areas when the tunnel is situated close to a foundation. Moreover, tunneling exerts a considerable effect on the foundations of nearby buildings, even in the case of deep underground tunnels (Shahin, et al., 2016).

(Button, et al., 2004) discussed digging two shallow tunnels through a thrust mélange, a challenging geological setting. It emphasizes the necessity of ongoing geological and geotechnical characterization in conjunction with sophisticated monitoring methods in order to comprehend the internal structure of the mélange and how it affects excavation. Key characteristics that characterize the behavior of the rock mass are identified with the aid of the acquired data. An illustration of data monitoring while construction is underway is shown in Figure 2-8 .

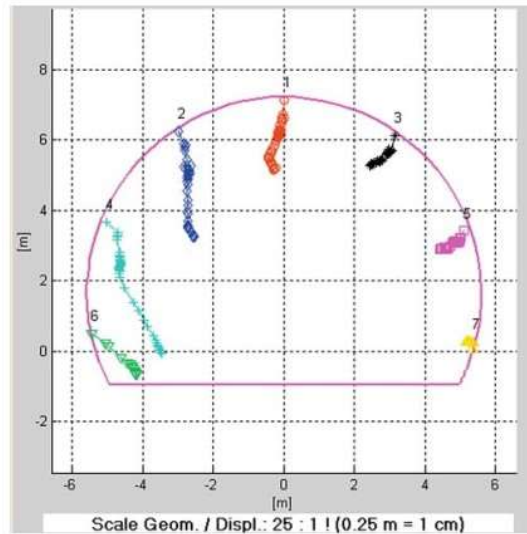


Figure 2-8 station 1,779 south bore Spital tunnel; displacements in a block impacted by the monitored displacements. Changes are amplified by 25 (Button, et al., 2004).

3. Numerical Modeling

3. Analysis of Shallow Tunneling in Bimrocks

This chapter presents the analysis of a shallow tunnel situated within a bimrock formation. The tunnel is characterized by a diameter of 10 meters and a depth of 20 meters.

The (Napoli, et al., 2018) stochastic technique, implemented in a Matlab routine through Monte Carlo simulations, was used to obtain a random distribution of rock blocks within the slope. To be more precise, variable block shape, eccentricity, location, size, orientation, and VBP were considered.

The coordinates and size of the ellipses representing the blocks (an eccentricity range of 0.4 to 0.9 was taken into account) were generated (as a Matlab output) for each VBP analyzed as a.txt file (Napoli, et al., 2018). This output was essential for the AutoCAD drawing of the tunnel and external boundaries of the models. Subsequently a .dxf file of the tunnel models was produced to be finally imported into the RS2 code from Rocscience for the numerical Finite Element analysis.

RS2 is used to analyze geotechnical constructions in two dimensions for mining and civil applications. RS2, which stands for "Rock and Soil 2-dimensional analysis program," is a multipurpose finite element analysis program that can be used for a variety of purposes, including tunnel and support design, groundwater seepage, consolidation, slope stability, embankments, dynamic analysis, foundations, and underground and surface excavation (Inc, 2024).

3.1. Numerical models arrangements

Ten distinct configurations for each VBP analyzed were generated through the MATLAB code to obtain robust statistical results. A matrix-only configuration was also considered, in order to compare the results.

Figure 3-1 illustrates examples of tunnel models with VPB equal to 25%, 40% and 55%. All the configurations used in this work are reported in the Appendix.

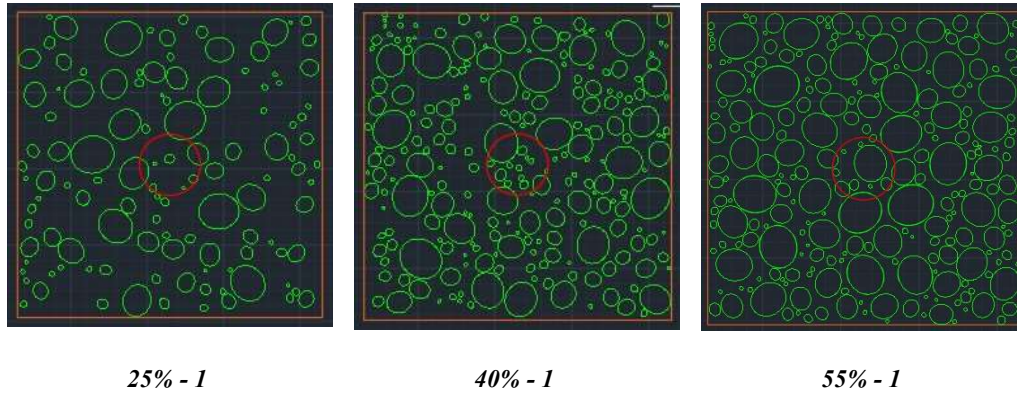


Figure 3-1 Example of different block arrangements for VBP in the range 25%-55%. The tunnel is represented by the red circle.

3.2. Material properties

Table 3-1 shows the material parameters that are taken into consideration according to (Napoli, et al., 2021).

Table 3-1 Designated Material Characteristics.

Property	Matrix	Blocks
Density ρ [kg/m ³]	2200	2700
Young's Modulus E [MPa]	40	40700
Peak Cohesion c [MPa]	0.065	11
Peak friction Angle ϕ [°]	28	50
Peak Tensile Strength [MPa]	0.02	6
Poisson ratio ν [-]	0.3	0.3
Uniaxial Compressive strength [MPa]	0.22	60

3.3. RS2 Modeling

As depicted in Figure 3-2, the modeling comprises three components: a bimrock section measuring 50×50 meters, a circular tunnel with a diameter of 10 meters (located in the center of the bimrock section), and the remaining area consisting of homogeneous soil (170×80 m). The vertical distance from the tunnel crown to the ground surface is 20 meters to meet the criteria for shallow tunnels.

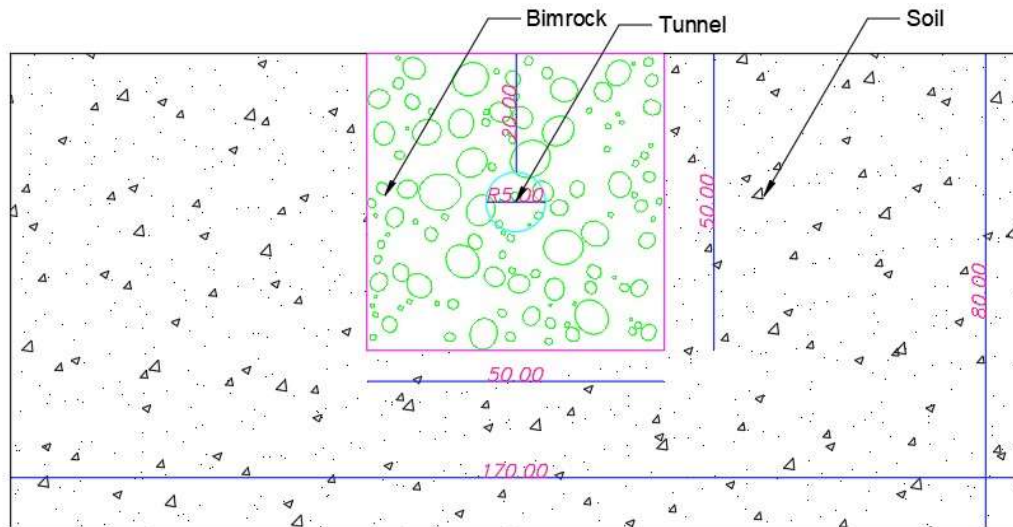


Figure 3-2 Numerical model dimensions (dimensions are in meters)

In order to simulate the gradual stress release resulting from material extraction during the excavation process, stress levels within the tunnel contour have to be diminished progressively. In RS2, this is achieved by activating the Factor load command, which systematically reduces the stresses at the nodes along the tunnel contour according to the specified reduction factors. Therefore, in the evaluation of excavation stages (analysis→ project setting: we could define stages which are shown in Figure 3-3), twelve distinct phases have been established to account for the load factor throughout the entire excavation process. This load factor begins at 1 and ultimately decreases to 0 upon the completion of the excavation. Table 3-2 illustrates the defined stages.

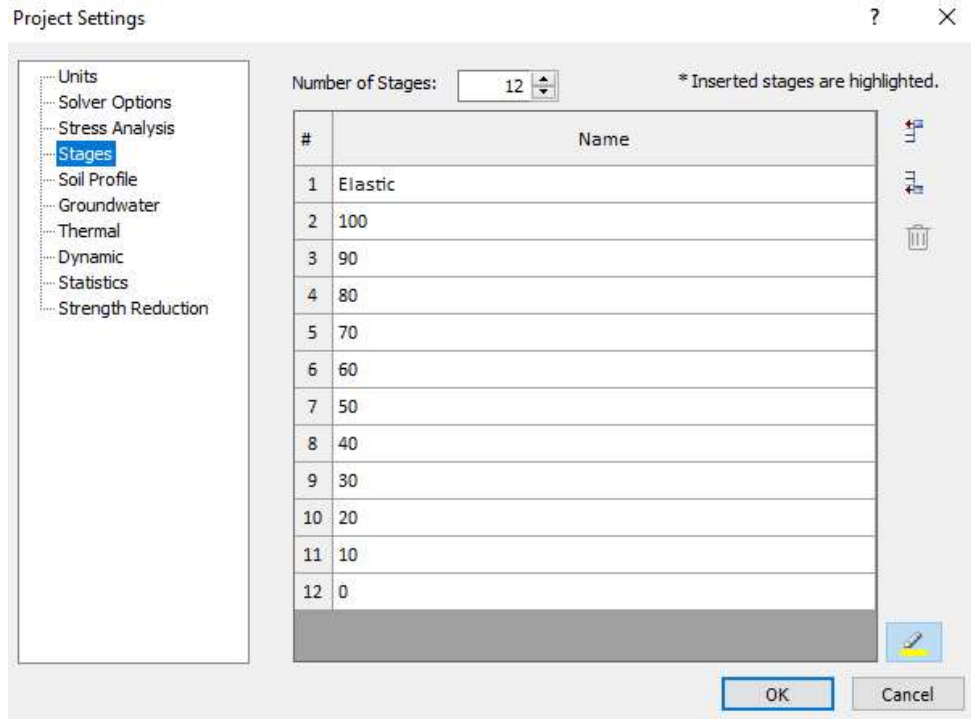


Figure 3-3 Defined Stages

Table 3-2 Defined Stages

Stage	Factor load
1	0
2	1
3	0.9
4	0.8
5	0.7
6	0.6
7	0.5
8	0.4
9	0.3
10	0.2
11	0.1
12	0

Material properties have been characterized for both elastic and plastic stages, as illustrated in Figure 3-4. It is evident that five distinct materials have been identified to represent various stages. The elastic soil is designated for the exterior of the bimrock box, while the elastic matrix and block are utilized during the initial phase prior to excavation. In subsequent stages, the focus shifts to the matrix and block to account for plastic behavior.

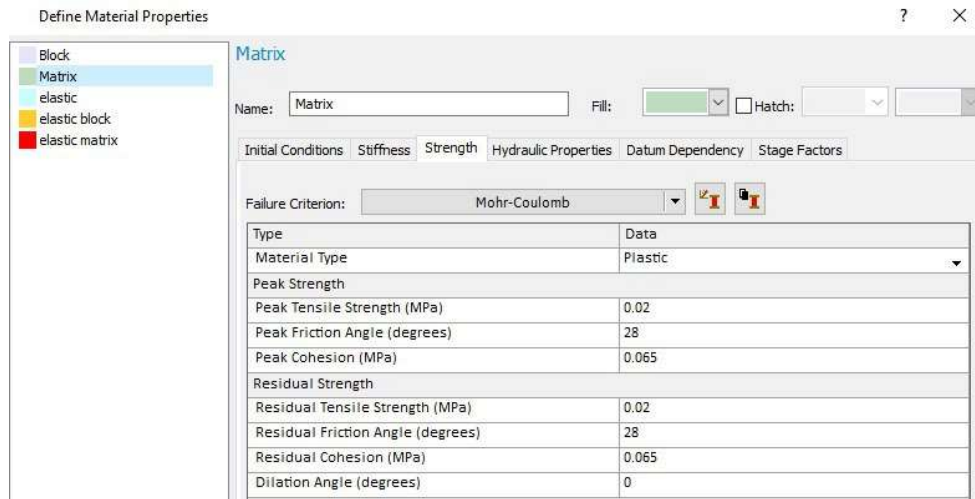


Figure 3-4 Define material properties

Field stress must be specified as gravity in the field stress characteristics menu in order to account for the soil load above the tunnel, depending on density. This procedure is depicted in Figure 3-5.

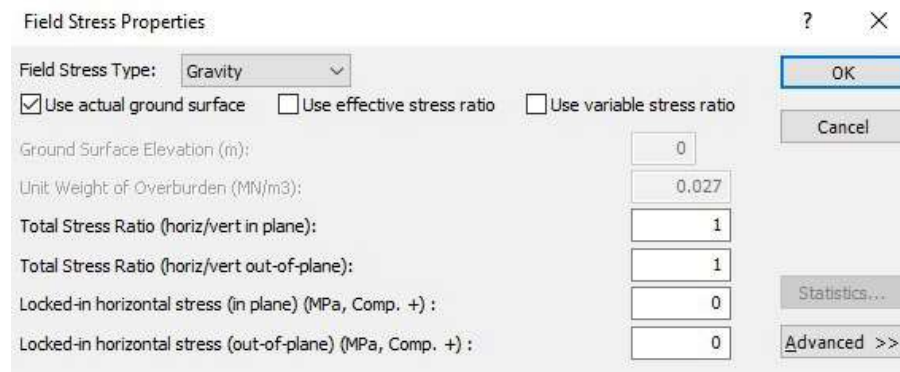


Figure 3-5 Field stress properties

A six-node triangular element type has been selected for generating the mesh, enhancing the speed and accuracy of the analysis (Figure 3-6).

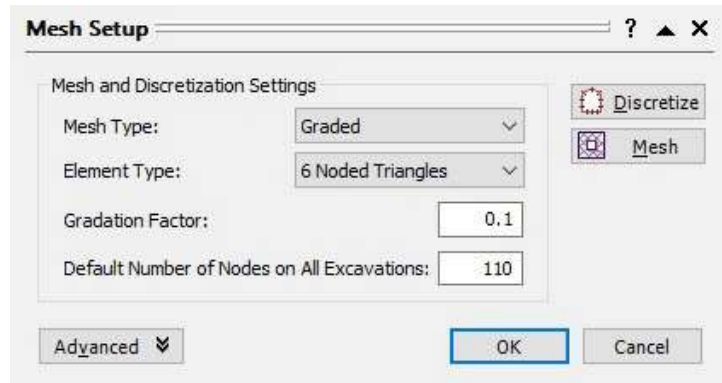
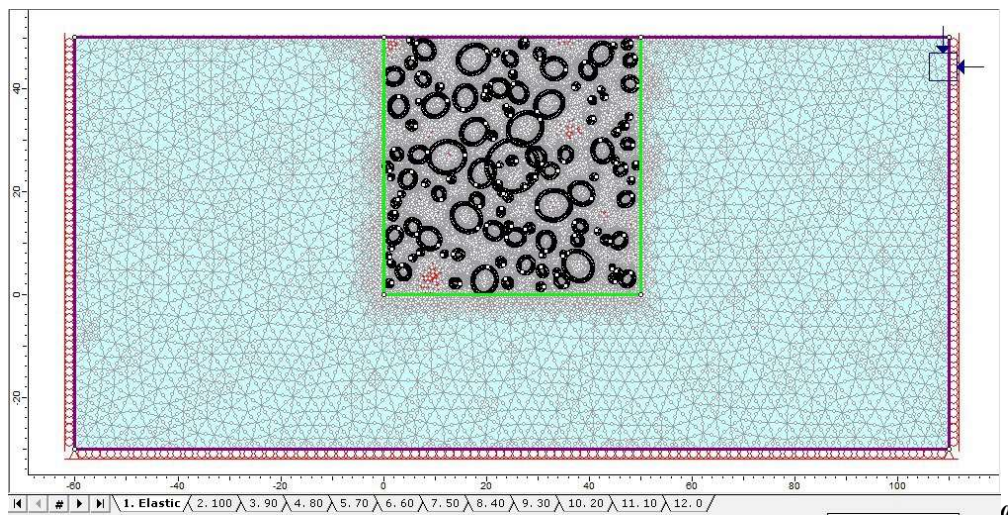


Figure 3-6 Mesh setup

Figure 3-7 depicts the final model prior to excavation and at the initial phase of excavation following the application of mesh. The soil is constrained in both the X and Y directions through the application of roller supports which are positioned on the right and left sides, as well as at the bottom, of the model, while remaining unrestrained at the ground level.



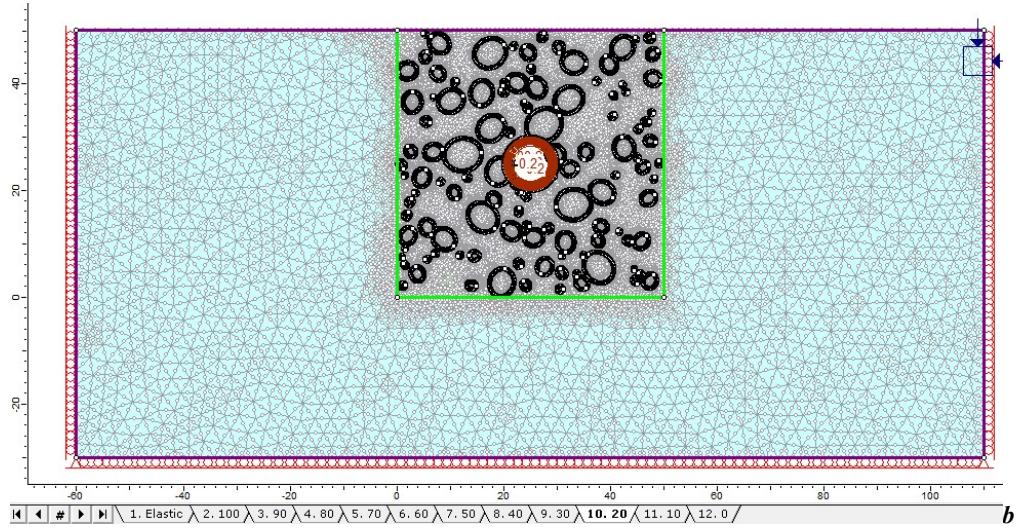


Figure 3-7 The final modeling: (a) before excavation, (b) stage tenth of excavation

3.4. Results

3.4.1. Vertical displacement

One model with matrix material and no blocks (i.e. VBP=0%) is analyzed in order to compare the results provided by the various heterogeneous tunnel models. The displacements at the ground level obtained above the tunnel are shown in Figure 3-8.

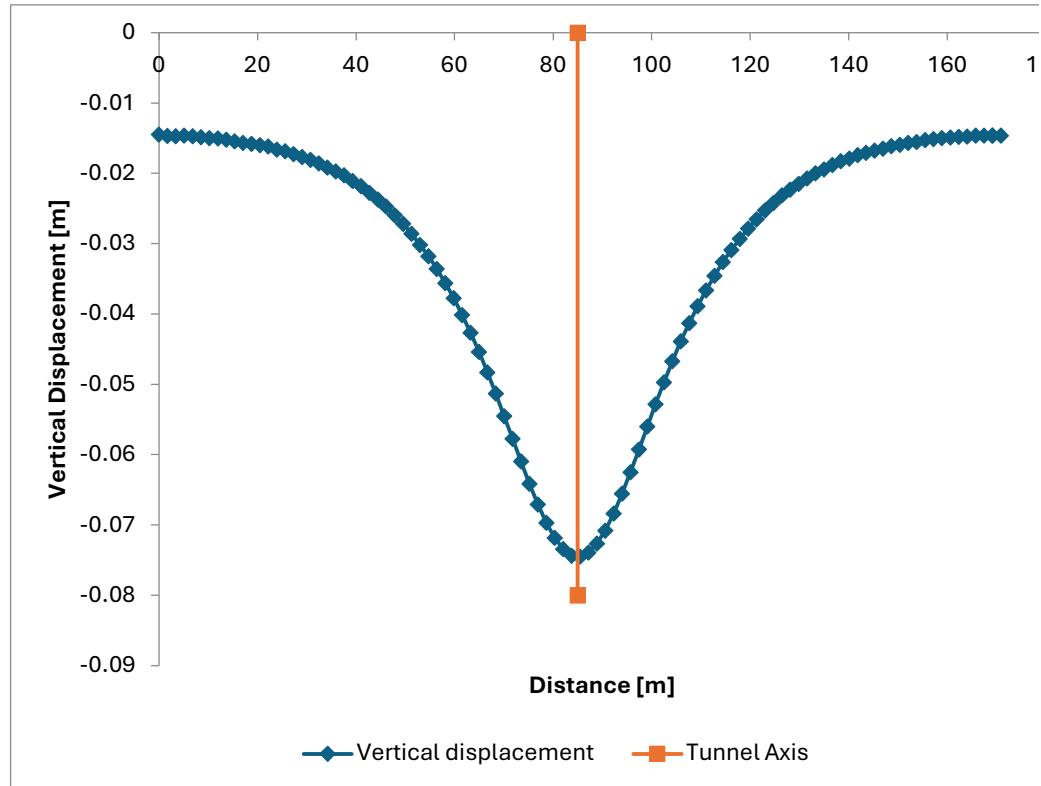


Figure 3-8 vertical displacement on the ground Surface (m), Matrix-only

According to Figure 3-8, a maximum vertical displacement of 7.4 cm occurs on the surface in correspondence of the tunnel axis.

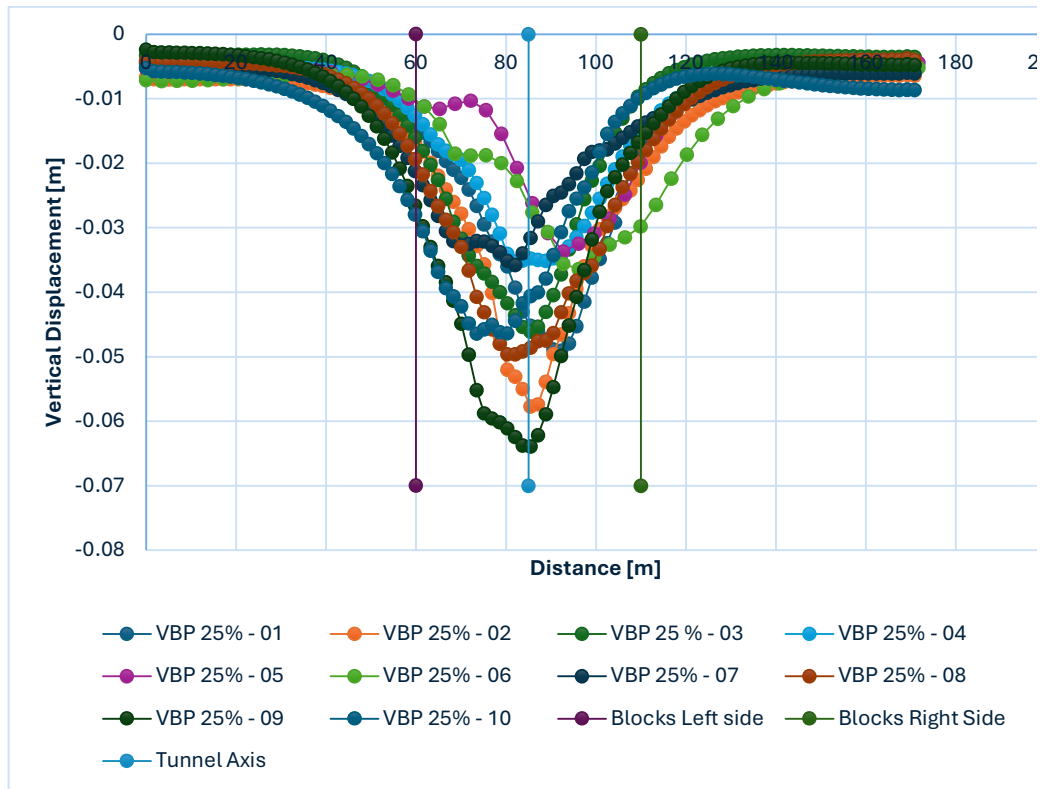


Figure 3-9 vertical displacement on the ground Surface (m), 25% VBP

Figure 3-9 illustrates the vertical displacement observed in the ten distinct configurations generated and analyzed for VBP 25%. The vertical lines indicate the left and right sides of the bimrock section and the tunnel axis location. The results obtained clearly indicate that the displacements are influenced by both the size of the blocks and their arrangement. In fact, differently from the matrix-only results displacements do not consistently align with the axis of the tunnel and are often asymmetrical. The highest recorded displacement is lower than that obtained in the VBP 0% model, occurs in the VBP 25%-09 configuration, and reaches 6.4 cm at the axis of the tunnel.

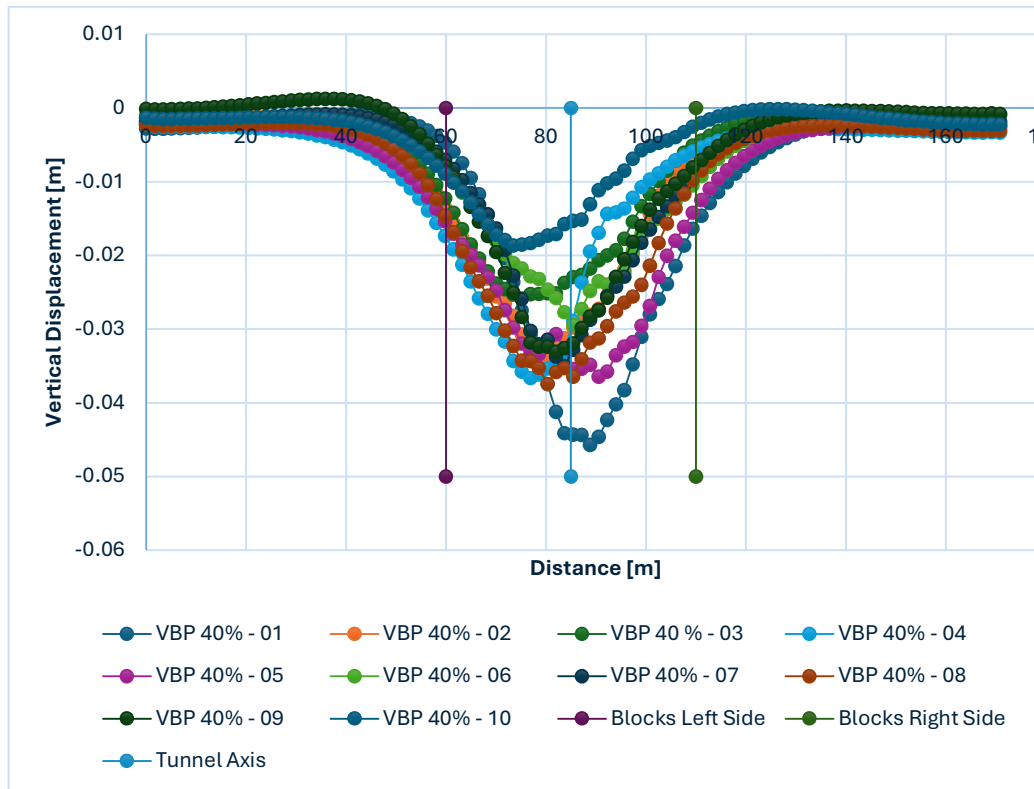


Figure 3-10 vertical displacement on the ground Surface (m), 40% VBP

The vertical displacements obtained from the ten configurations at VBP 40% models are illustrated in Figure 3-10. The data suggest that the displacements diminish as the percentage of blocks increases, and that the maximum displacement does not occur at the tunnel axis but depends on the spatial distribution of the different sized blocks. The maximum displacement recorded is found in the VBP 40%-01 configuration, which measures approximately 4.5 cm, close to the tunnel axis.

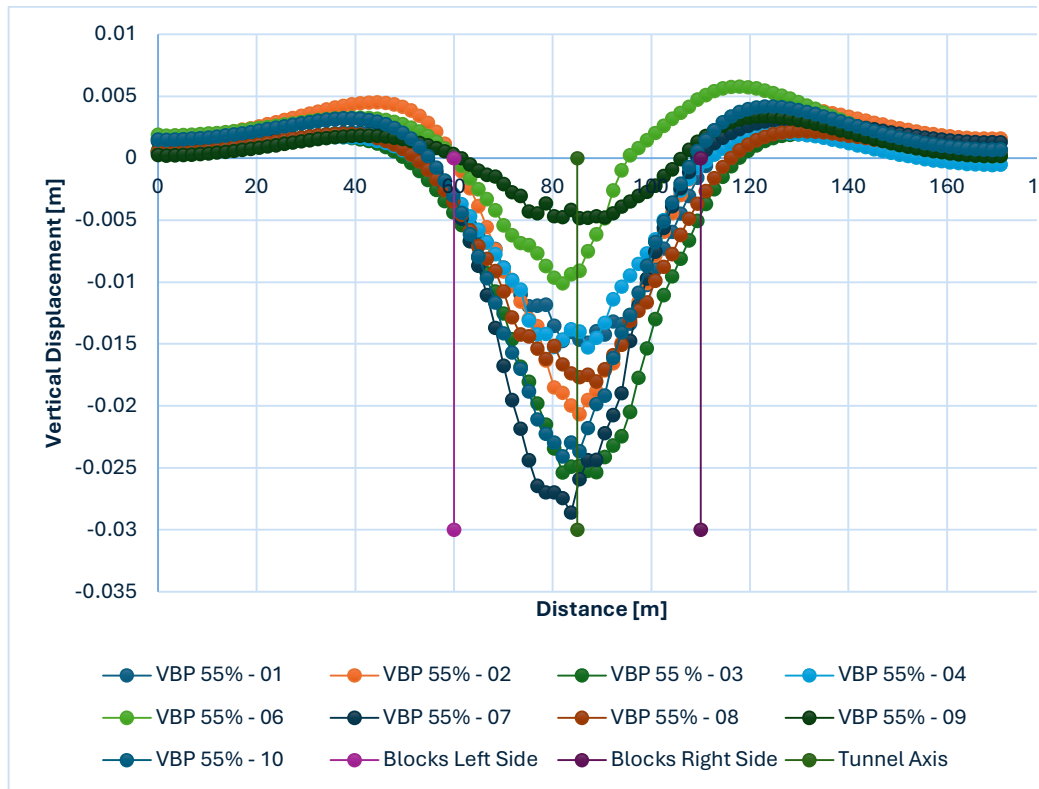


Figure 3-11 vertical displacement on the ground Surface (m), 55% VBP

The vertical displacement patterns of the models with a VBP of 55% are depicted in Figure 3-11. Maximum displacements are generally observed along the tunnel axis, with the exception of configurations 06 and 09. Additionally, a minor uplift is noted outside the tunnel area. The highest recorded displacement occurs in the VBP 55%-01 configuration near the tunnel axis, measuring approximately 2.8 cm. The maximum uplift was observed in VBP 55%-06, measuring 5 mm. This phenomenon, observed mainly beyond the bimrock zone, is commonly found in numerical analyses when the same value of the elastic modulus is considered for both loading and unloading processes. In this case, the higher stiffness of the bimrock area with respect to that of the surrounding soil compels the outward transfer of stress, amplifying this problem and prompting a slight upward movement in the adjacent ground.

Summing up, the results obtained from the numerical simulations indicate that by increasing VBP within the range of 25 to 55 percent, the maximum shallow vertical displacements in the area affected by the excavation are reduced by approximately 13.51%, 39.19%, and 62.16% for VBP levels of 25%, 40%, and 55%, respectively. The

distribution of the displacements is influenced by the size and location of the blocks inside the matrix.

Table 3-3 Maximum displacement and it's variations in different models

VBP%	Maximum displacement (cm)	Variation related to VBP 0 %
0	7.4	-
25	6.4	-13.51%
40	4.5	-39.19%
55	2.8	-62.16%

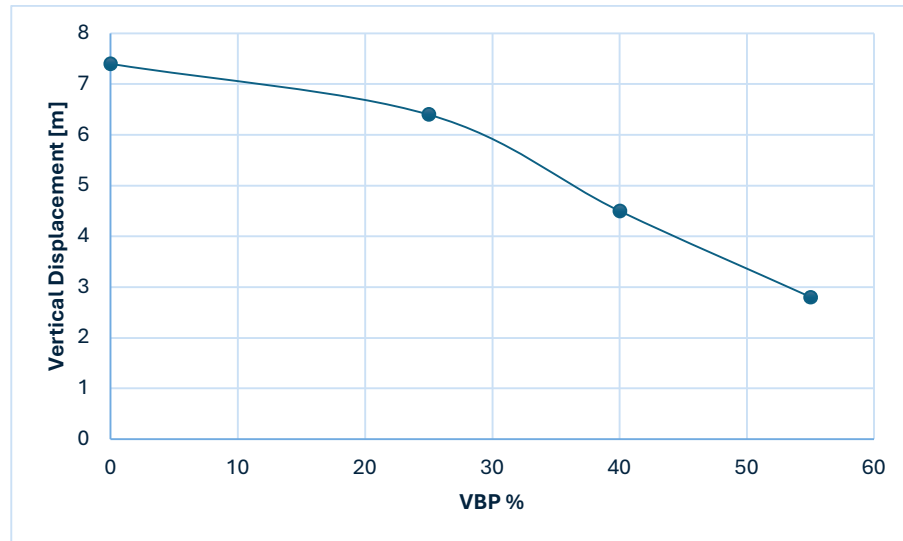


Figure 3-12 vertical displacement versus VBP %

3.4.2. Yielded elements

The results reported in Figure 3-13, indicate that as the VBP increases, the material's stiffness rises because of the greater proportion of rigid blocks. This results in a shift in the distribution of the applied load, with the blocks bearing more of the load, which in turn reduces the deformation in the matrix. As a result, fewer matrix elements reach the yield point, as the material overall experiences less deformation. Thus, the number of yielded elements decreases as VBP increases, due to the material becoming more rigid and constrained.

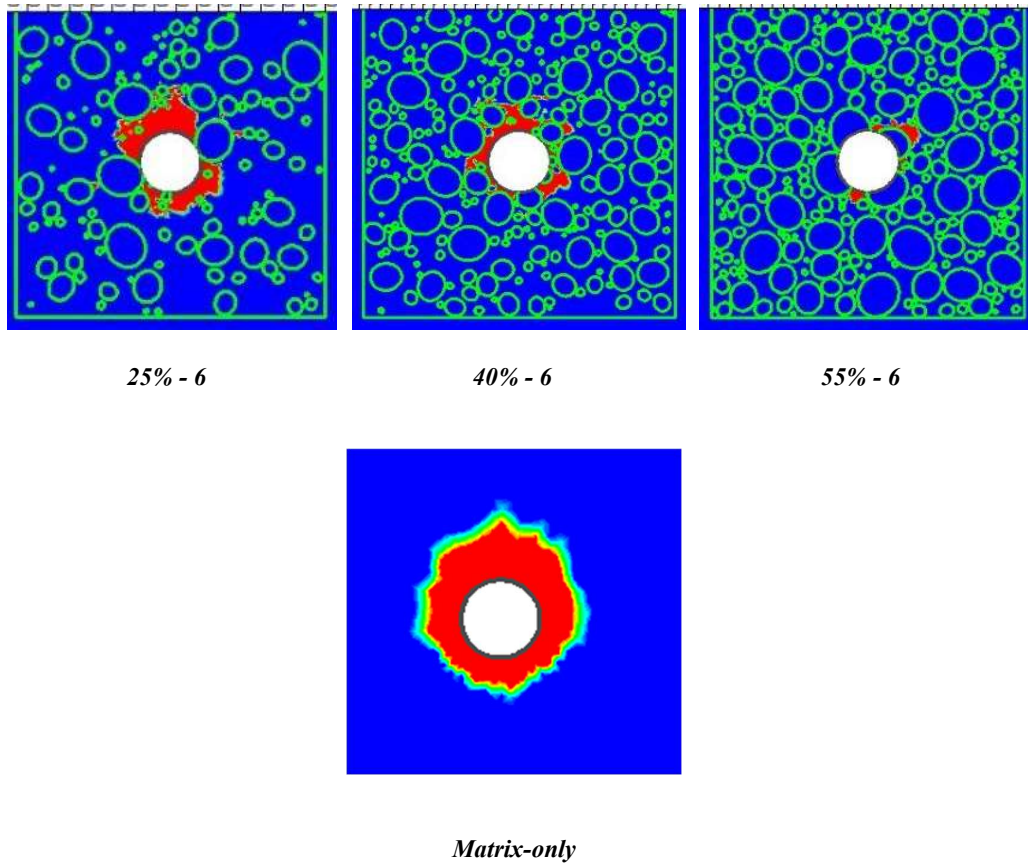
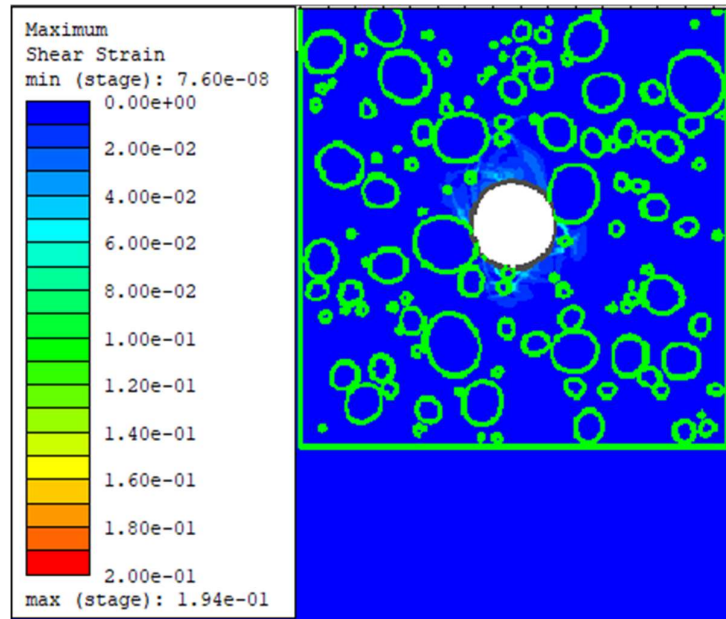


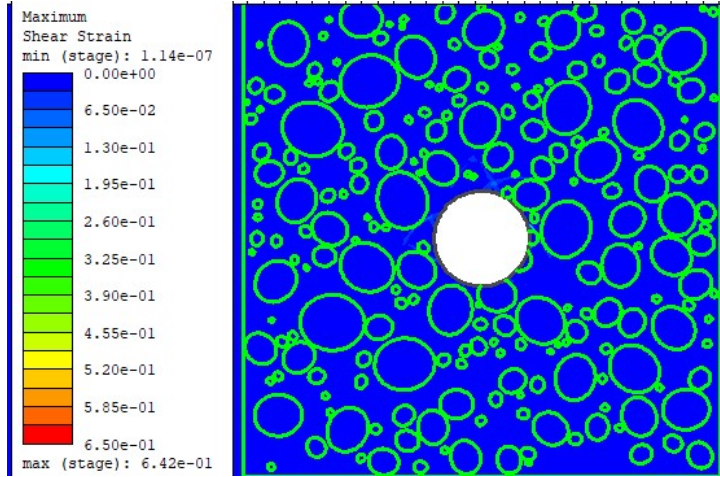
Figure 3-13 Yielded elements

3.4.3. Maximum shear strain

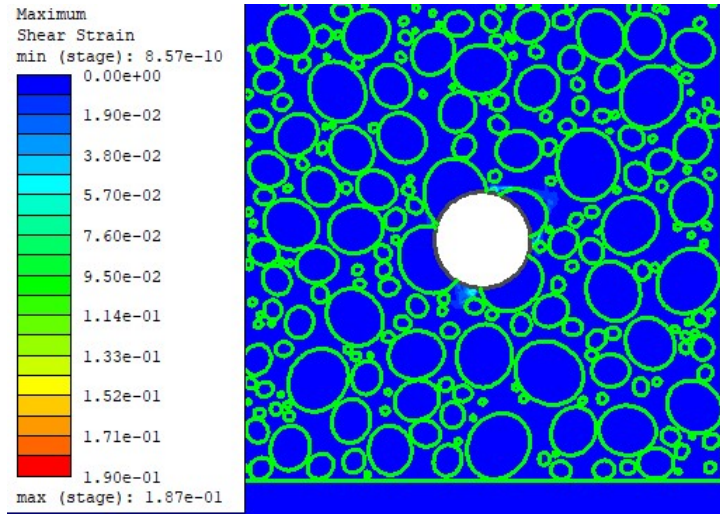
The data presented in Figure 3-14 shows at VBP 25%, the material is more deformable, allowing for more uniform deformation and lower shear strain due to fewer rigid blocks that result in less stress concentration. At 40% VBP, there is an ideal balance between the deformability of the matrix and the concentration of rigid blocks, which causes the highest shear strain as stress becomes concentrated and deformation localizes in the matrix. At 55% VBP, the material becomes stiffer due to the increased number of rigid blocks, restricting matrix deformation and leading to a decrease in shear strain. This observation indicates that the worst distribution of blocks which maximize the concentration of shear strain is at an intermediate VBP value.



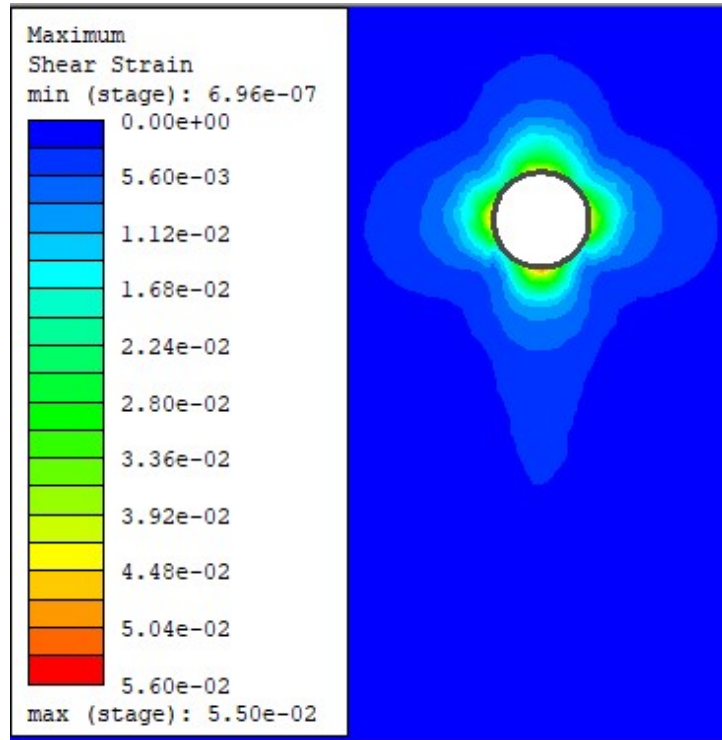
25% - 6



40% - 6



55% - 6

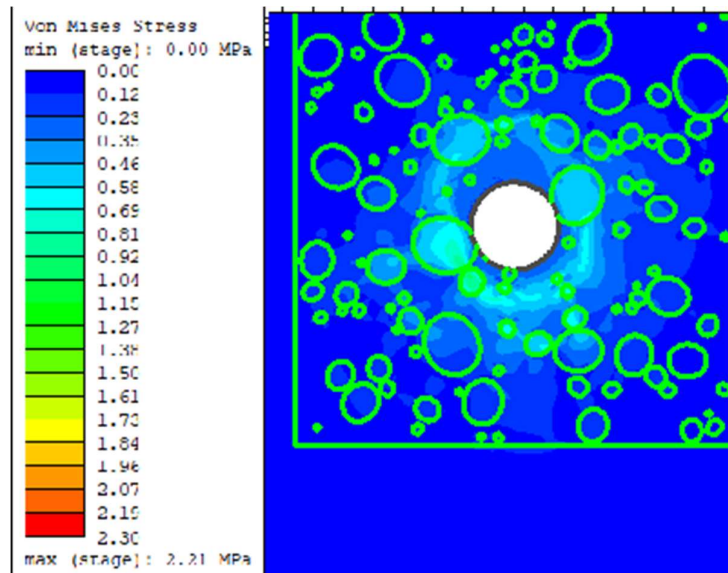


Matrix-only

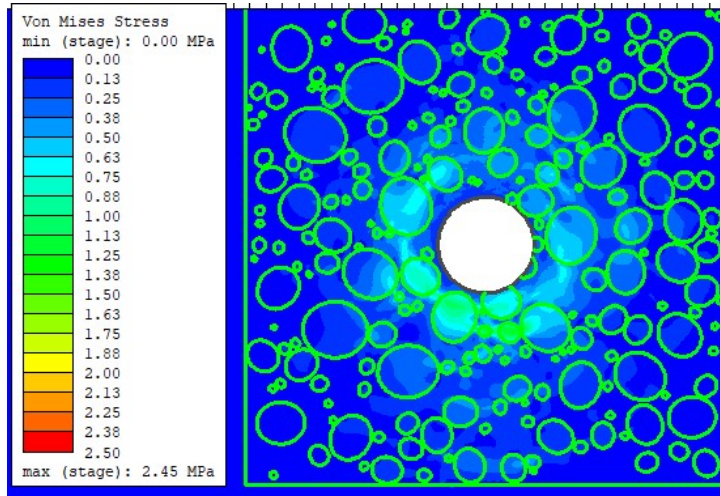
Figure 3-14 Maximum shear strain

3.4.4. Von Mises Stress

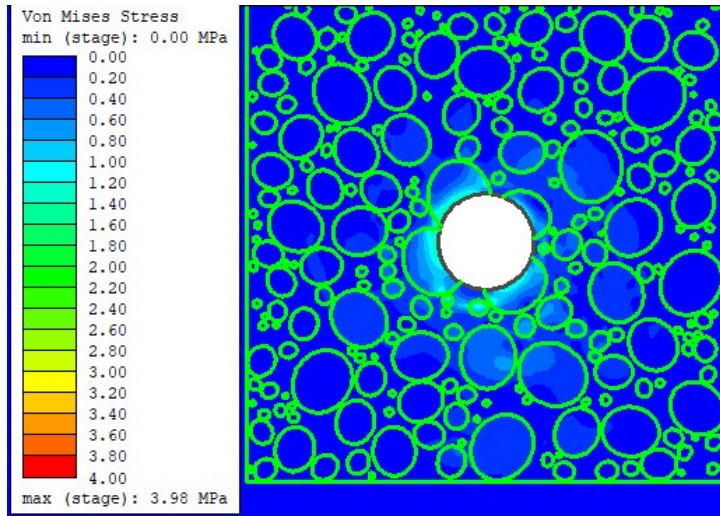
The analysis presented in the Figure 3-15 indicates that an increase in the VBP results in a corresponding rise in Von Mises stress. This phenomenon can be attributed to several interrelated factors, including enhanced material stiffness and the concentration of stress around the rigid blocks. The introduction of additional rigid blocks modifies the deformation characteristics, consequently resulting in elevated localized stress levels.



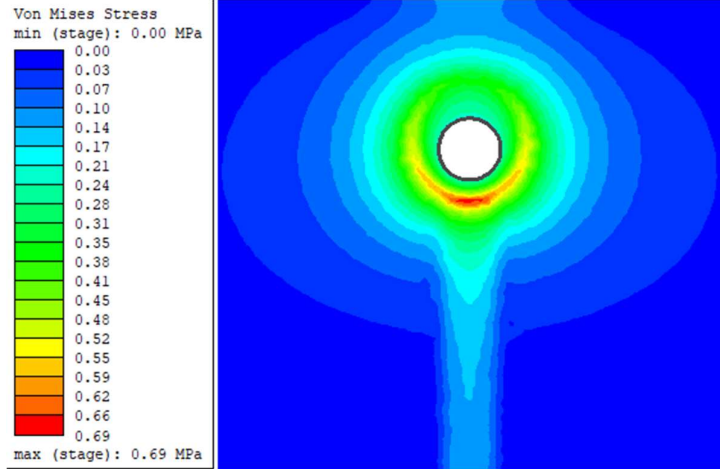
25% - 6



40% - 6



55% - 6



Matrix-only

Figure 3-15 Von Mises Stress

3.5. Conclusion

This research offers significant insights into the ground vertical displacements and the strains and stresses around shallow tunnels excavated within block-in-matrix rocks (bimrocks), particularly focusing on the role of the Volumetric Block Proportion (VBP) on the processes induced. A number of numerical simulations have been carried out, by using the Finite Element Method implemented in RS2 (Rocscience). The study reveals that an increase in VBP leads to a marked decrease in vertical displacements and an increase of their nonuniformity.

Numerical modeling showed that an increase in VBP results in a reduction of the vertical ground displacements of 62.16% as VBP increases from 0% to 55%. This observation supports the statement that the inclusion of rigid blocks into the matrix contributes to the stability of the ground above the tunnel.

Moreover, the results indicate that the distribution of the vertical displacements at the ground level does not follow the classical Gaussian shape, centered to the tunnel axis, but it is influenced by the location and the size of the blocks. For higher percentages of blocks, the pattern of displacement becomes more regular and similar to that of the homogeneous material (only matrix).

These findings highlight the importance of accounting for bimrock heterogeneity in tunnel design, particularly in urban settings where managing surface settlement is crucial.

Future investigations should focus on aspects such as block shape, matrix anisotropy, and the effects of dynamic loading to further refine predictive models and advance tunneling practices in complex geological formations.

Bibliography

Afifipour, M and Moarefvand, P. 2014. *Mechanical behavior of bimrocks having high rock block proportion.* Department of Mining and Metallurgy Engineering, Amirkabir University of Technology, Hafez 424, Tehran 15875 4413, Iran : International Journal of Rock Mechanics & Mining Sciences, Page 40-48, 2014.

Barbero, M; Bonini, M and Borri-Brunetto, M. 2008. *Three-Dimensional Finite Element Simulations of Compression Tests on Bimrock .* s.l. : The 12th International Conference of International Association for Computer Methods and Advances in Geomechanics (IACMAG), , 2008.

Barla, G and Pelizza, S . 2000. *TBM Tunnelling In Difficult Ground Conditions.* s.l. : ISRM International Symposium, Melbourne, Australia, 2000.

Button, E; Riedmüller, G; Schubert, W; Klima, K; Medley , E. 2004. *Tunnelling in tectonic melanges—accommodating the impacts of geomechanical complexities and anisotropic rock mass fabrics.* s.l. : Bulletin of Engineering Geology and the Environment, Volume 63, pages 109–117, 2004.

Chapman, D; Metje, N and Stärk, A. 2018. *Introduction to Tunnel Construction .* s.l. : Taylor & Francis Group, 2018.

Coli, N; Berry, P; Boldini, D; Bruno, R. 2011. *The contribution of geostatistics to the characterisation of some bimrocks properties.* s.l. : Engineering Geology, Page 53–63, 2011.

Cowan, DS. 1985. *Structural styles in Mesozoic and Cenozoic mélanges in the western Cordillera of North America.* s.l. : Department of Geological Sciences, University of Washington, Seattle, Washington 9819, 1985.

Hu, Y; Sun, S and Sun, Y . 2024. *An Experimental Investigation of the Effects of Block Proportion on Bimrocks, Considering Different Block-to-Matrix Strength Ratios.* Basel, Switzerland : mdpi, journal of materials, Vol 17, 1114, 2024.

Inc, Rocscience. 2024. *RS2 Tutorials Overview Version 11.* s.l. : Rocscience Inc, 2024.

Kahraman, S; Alber, M; Fener, M; Gunaydin, O. 2014. *An assessment on the indirect determination of the volumetric block proportion of Misis fault breccia (Adana, Turkey).* s.l. : Bulletin of Engineering Geology and the Environment, Volume 74, pages 899–907, 2014.

Kalender, A; Sonmez, H; Medley, E.W; Tunusluoglu, C; Kasapoglu, K.E. 2014. *An approach to predicting the overall strengths of unwelded bimrocks and bimsoils.* s.l. : Engineering Geology, Page 65-79, 2014.

Lindquist, E.S; Goodman, R. 1994. *Strength deformation properties of a physical model melange.* s.l. : Proceedings 1st North American Rock Mech, Symp., Austin, Texas, 843-850, 1994.

Lindquist, E.S. 1991. *Fractals-Fracture and Franciscan Melange, Term Paper for CE 280.* s.l. : Rock Mechanics instructor: Prof. R.E Goodman, Dept Civil Engineering, University of California, Berkeley., 1991.

Lindquist, E.S. 1994. *The strength and deformation properties of melange.* s.l. : University of California, Berkeley, A dissertation submitted in Doctor of Philosophy, 1994.

Medely, E.W. 1997. *Uncertainty in estimates volumetric proportions in melange bimrocks.* s.l. : Proceedings of International Symposium on Engineering Geology and the Environment, Athens, 23-27, Page 267-272, 1997.

Medley, E.W and Lindquist, E.S. 1995. *The enEngineering significance of the scale-independence of some Franciscan melanges in California, USA.* Reno, Nevada : The 35th U.S. Symposium on Rock Mechanics (USRMS), 1995.

Medley, E.W. 2001. *Estimating Block Size Distributions of Melanges and Similar Block-in Matrix Rocks (Bimrocks).* Toronto : Proceedings of 5th North American Rock Mechanics Symposium (NARMS), 2001. pp. 509-606.

Medley, E.W. 1999. *Systematic characterization of melange bimrocks and other chaotic soil/rock mixtures.* s.l. : Journal of Geomechanics and Tunneling, V 17, Page 152-162, 1999.

Medley, E.W. 1994. *The Engineering Characterization of Melanges.* s.l. : UNIVERSITY of CALIFORNIA at BERKELEY, California, PhD diss, 1994.

Najafvand, K; Khosravi, M.H; Amini, M; Medley, E.W. 2024. *Use of LBPs to estimate VBPs as observed from an investigation of physical model bimrocks.* s.l. : Bulletin of Engineering Geology and the Environment, Volume 83, article number 382, 2024.

Napoli, M.L; Barbero, M; Ravera, E; Scavia, C. 2018. *A stochastic approach to slope stability analysis in bimrocks. International.* s.l. : Journal of Rock Mechanics and Mining Sciences, 101, pp.41-49, 2018.

Napoli, M.L; Barbero, M and Scavia, C . 2021. *Tunneling in heterogeneous rock masses with a block-in-matrix fabric.* s.l. : International Journal of Rock Mechanics and Mining Sciences, Volume 138, 104655, 2021.

Napoli, M.L; Milan, L; Barbero, M; Medley, E.W. 2022. *Investigation of Virtual Bimrocks to Estimate 3D Volumetric Block Proportions from 1D Boring Measurements.* s.l. : Geosciences Journal, 12(11), 405, 2022.

Patil, M; Choudhury, D; Ranjith, P.G; Zhao, J. 2018. *Behavior of shallow tunnel in soft soil under seismic conditions.* s.l. : Tunnelling and Underground Space Technology, Volume 82, Pages 30–3, 2018.

Peitgen, H.O; Jürgens, H and Saupe, D. 1992. *Length, Area and Dimension: Measuring Complexity and Scaling Properties.* s.l. : Springer Science, Chaos and Fractals, V 4, Page 184-190, 1992.

Pinto, F and J. Whittle, A . 2013. *Ground Movements due to Shallow Tunnels in Soft Ground. I: Analytical Solutions.* s.l. : Journal of Geotechnical and Geoenvironmental Engineering, Volume 140, 2013.

Abdellah, R; Wael, M; Ali, A and Yang, H.S. 2018. *Studying the effect of some parameters on the stability of shallow tunnels.* s.l. : Journal of Sustainable Mining, Volume 17, Issue 1, Pages 20-33, 2018.

Raymond, L. 1984. *Classification of melanges*. s.l. : Geological society of America, Appalachian state University, 1984.

Shahin, H.M; Nakai, T; Ishii, K; Iwata, T; Kuroi, S. 2016. *Investigation of influence of tunneling on existing building and tunnel: model tests and numerical simulations*. s.l. : Acta Geotechnica, Volume 11, pages 679–692, 2016.

Sharafisafa, M; Aliabadian, Z; Sato, A; Shen, L. 2024. *Effect of strain rate on the failure of bimrocks using the combined finite-discrete element method*. 2024. Computers and Geotechnics, Volume 176, 106712.

Tien, Y.M; Lu, Y.C and Chung, Y.J. 2010. *Uncertainty In Estimation of Volumetric Block Proportion of Bimrocks By Using Scanline Method*. s.l. : 44th U.S. Rock Mechanics Symposium and 5th U.S.-Canada Rock Mechanics Symposium, Salt Lake City, Utah, 2010.

Turcotte, D.L. 1986. *Fractals and Fragmentation*. s.l. : JOURNAL OF GEOPHYSICAL RESEARCH, VOL. 91, NO. B2, PAGES 1921-192, 1986.

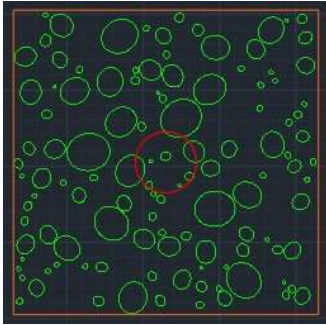
Yazdani, A; Karimi-Nasab, S and Jalalifar, H . 2024. *Shear behavior and dilatancy of an artificial hard-matrix bimrock: An experimental study focusing on the role of blocky structure*. s.l. : Rock Mechanics Bulletin Volume 3, 100149, 2024.

Zhang, Z.L; Xu, W.J; Xia, W; Zhang, H.Y. 2016. *Large-scale in-situ test for mechanical characterization of soil–rock mixture used in an embankment dam*. s.l. : International Journal of Rock Mechanics & Mining Sciences, Vol 17, Page 317-322, 2016.

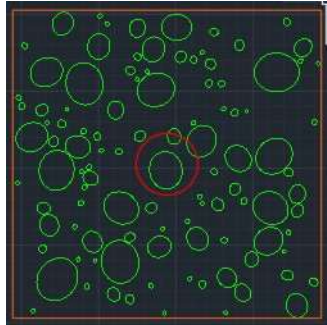
Zhou, H; Zhang, C ; Li, Z; Hu, D; Hou, J. 2014. *Analysis of mechanical behavior of soft rocks and stability control in deep tunnels.* s.l. : Journal of Rock Mechanics and Geotechnical Engineering 6, Pages 219-226, 2014.

Appendix

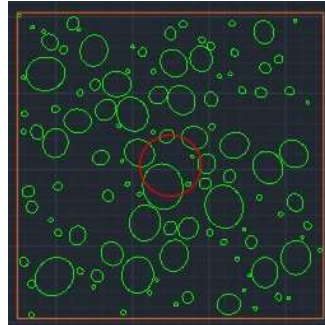
VBP arrangements



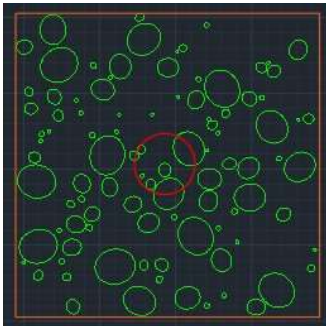
25% - 1



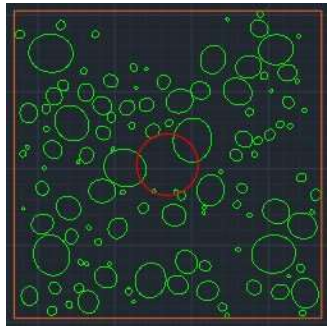
25% - 2



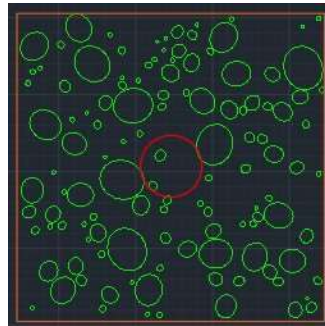
25% - 3



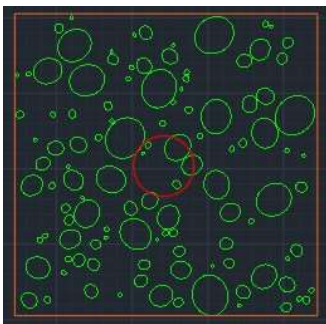
25% - 4



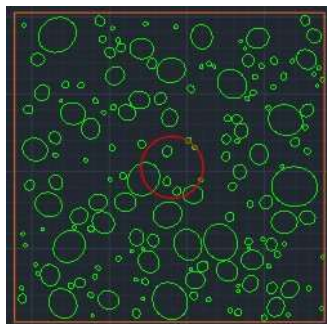
25% - 5



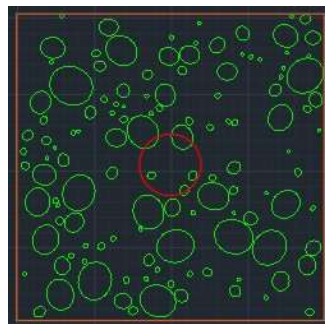
25% - 6



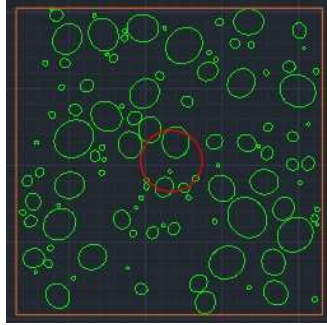
25% - 7



25% - 8

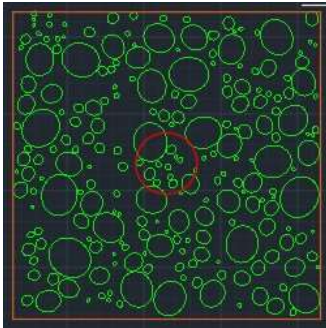


25% - 9

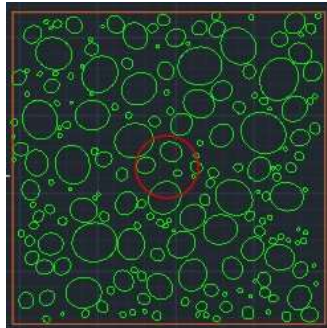


25% - 10

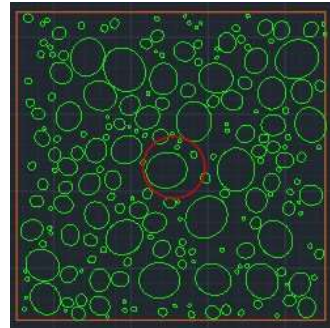
Arrangements of 25% VBP



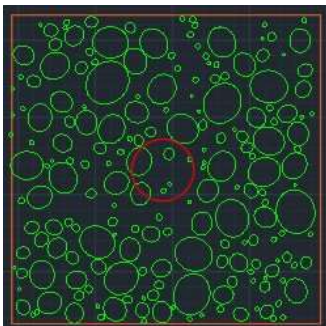
40% - 1



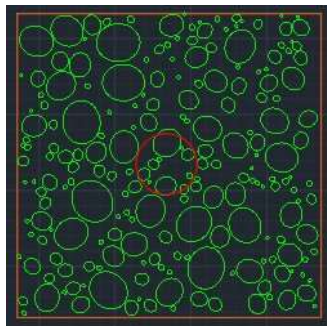
40% - 2



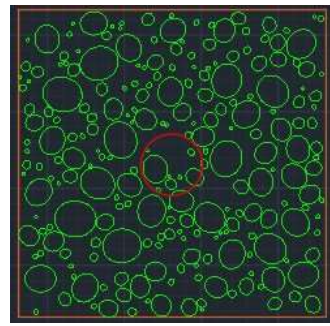
40% - 3



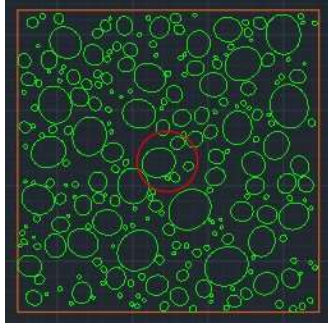
40% - 4



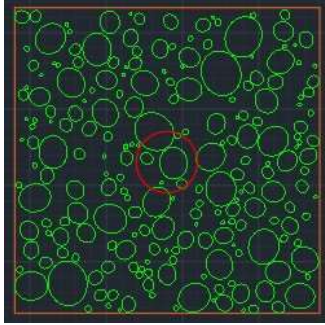
40% - 5



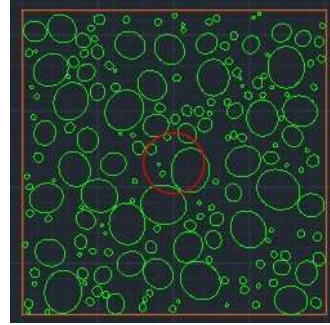
40% - 6



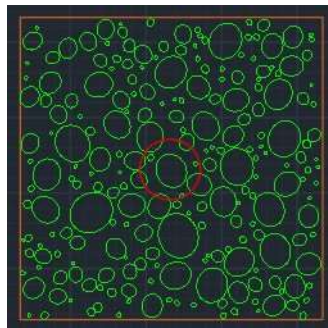
40% - 7



40% - 8

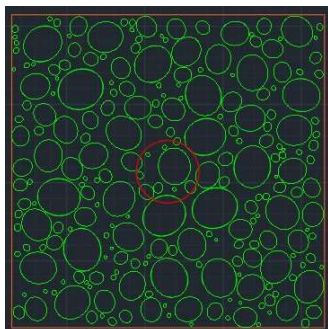


40% - 9

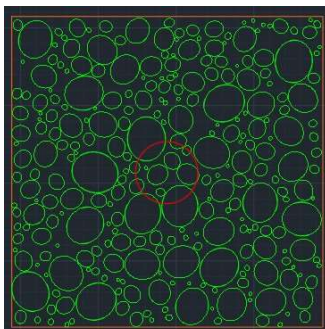


40% - 10

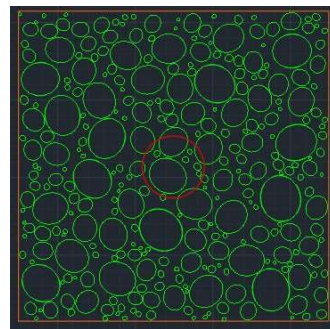
Arrangements of 40% VBP



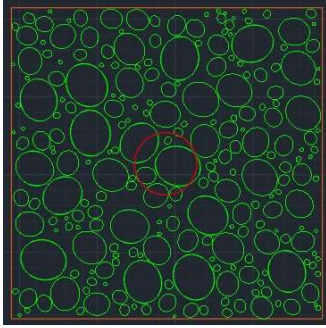
55% - 1



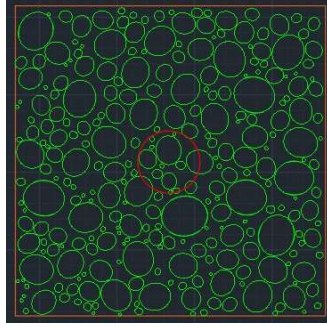
55% - 2



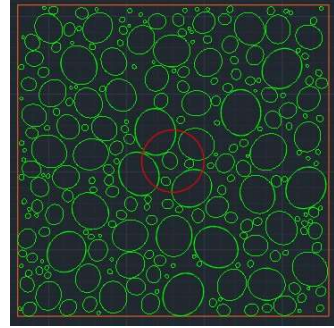
55% - 3



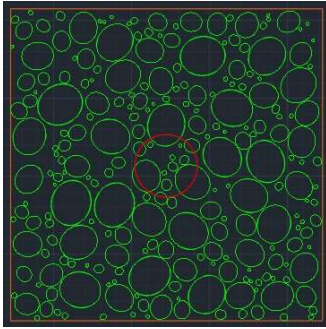
55% - 4



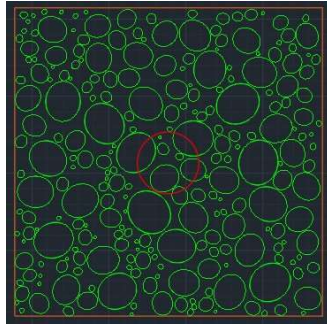
55% - 5



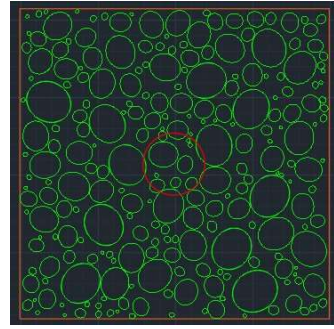
55% - 6



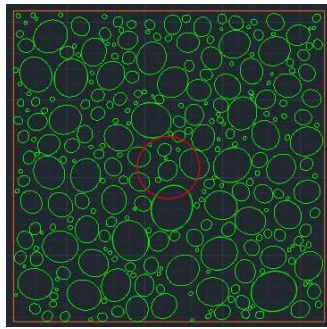
55% - 7



55% - 8



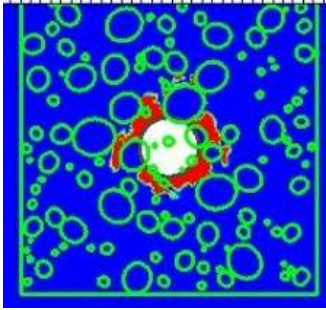
55% - 9



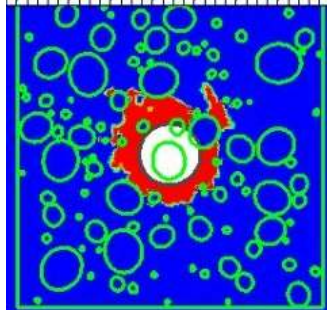
55% - 10

Arrangements of 55% VBP

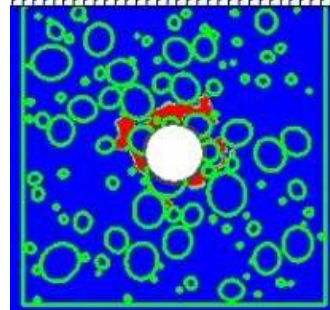
Yielded Elements



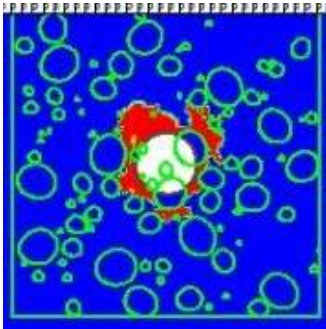
25% - 1



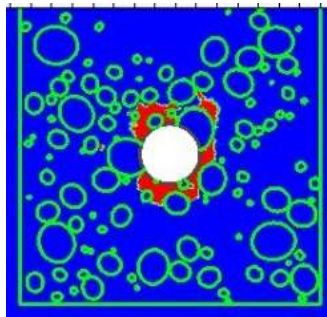
25% - 2



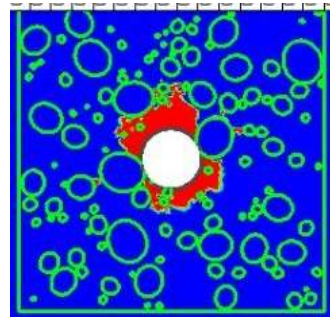
25% - 3



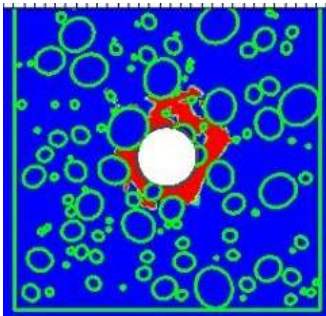
25% - 4



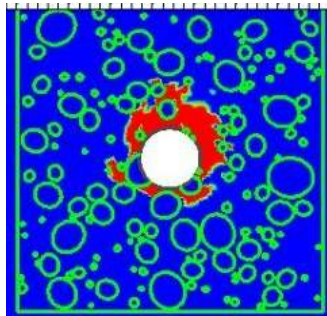
25% - 5



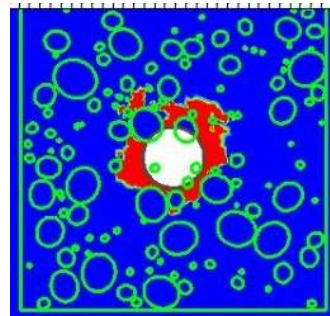
25% - 6



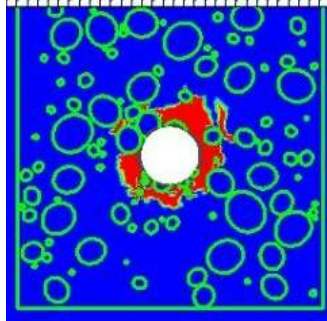
25% - 7



25% - 8

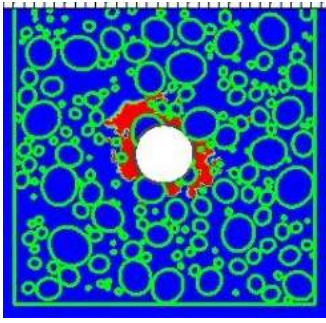


25% - 9

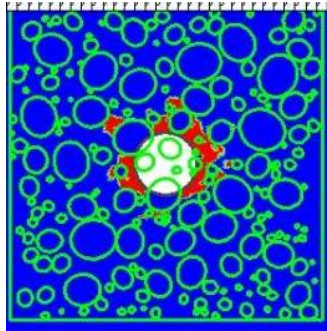


25% - 10

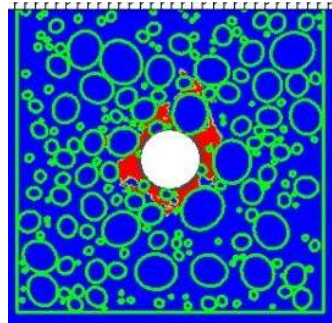
Yielded Elements of 25% VBP



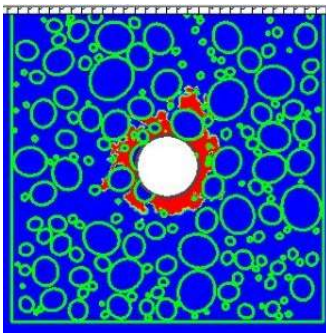
40% - 1



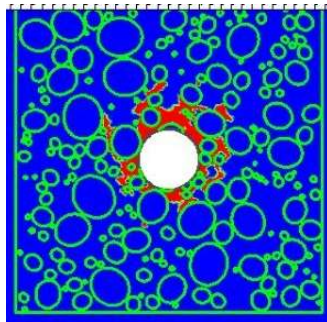
40% - 2



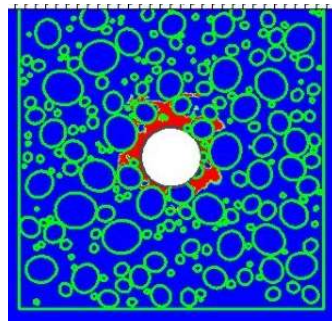
40% - 3



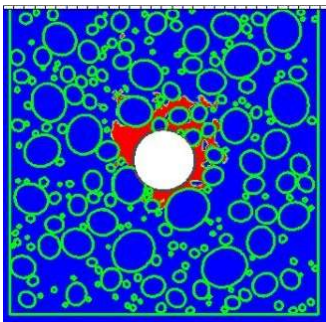
40% - 4



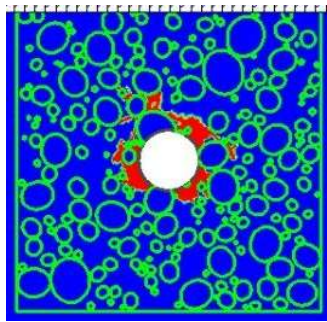
40% - 5



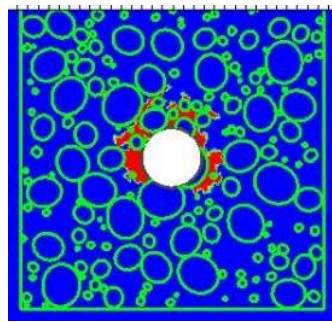
40% - 6



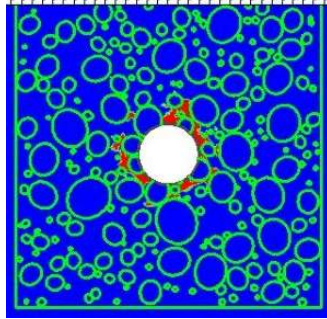
40% - 7



40% - 8

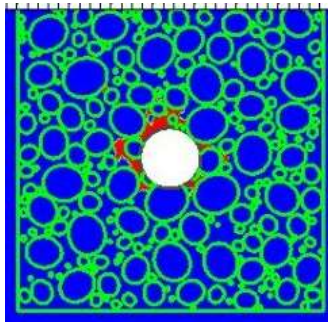


40% - 9

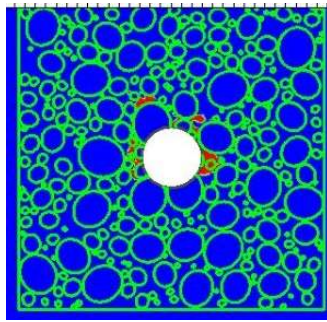


40% - 10

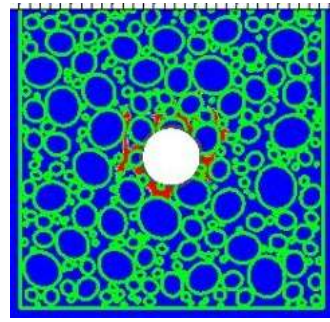
Yielded Elements of 40% VBP



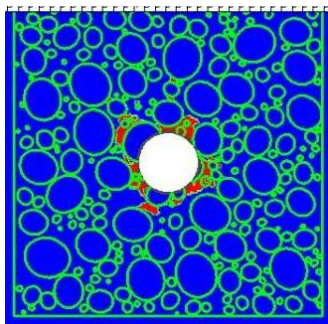
55% - 1



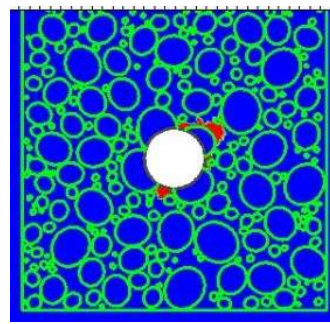
55% - 2



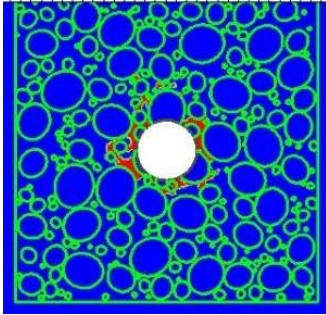
55% - 3



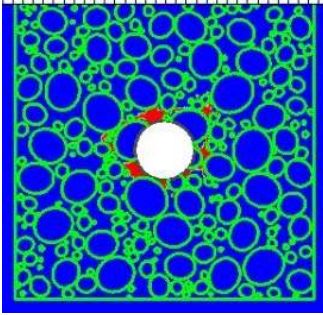
55% - 4



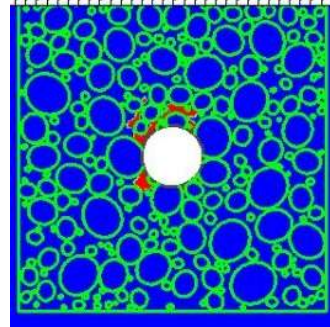
55% - 6



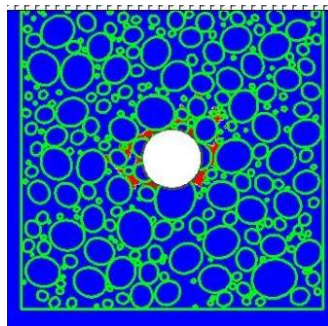
55% - 7



55% - 8



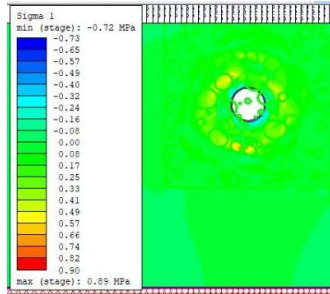
55% - 9



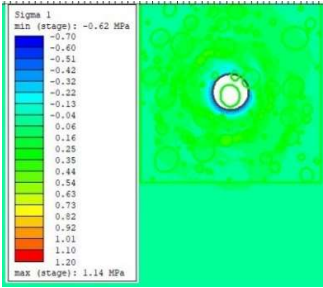
55% - 10

Yielded Elements of 55% VBP

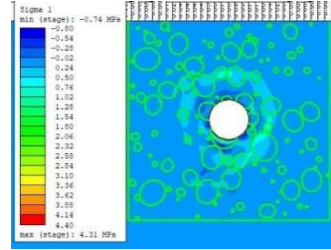
Maximum Stress (σ_1) contours



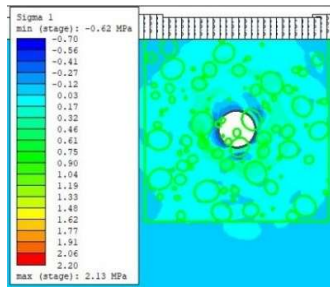
25% - 1



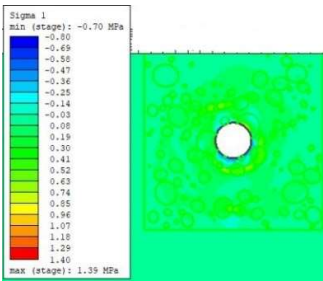
25% - 2



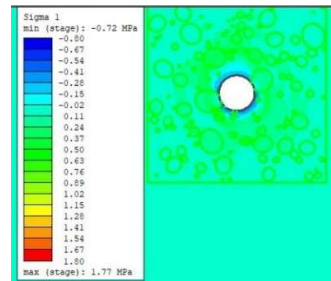
25% - 3



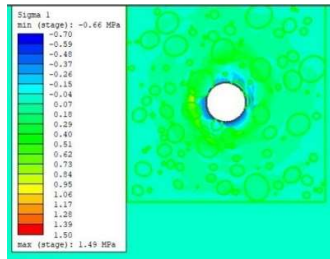
25% - 4



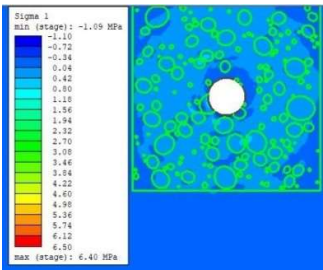
25% - 5



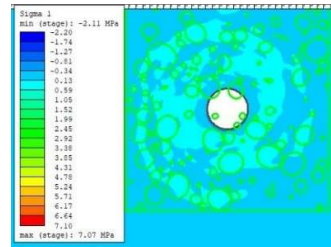
25% - 6



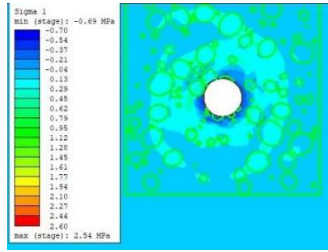
25% - 7



25% - 8

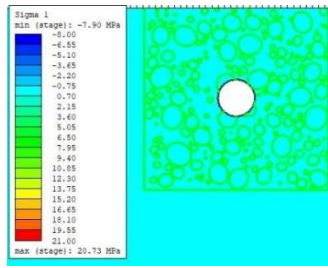


25% - 9

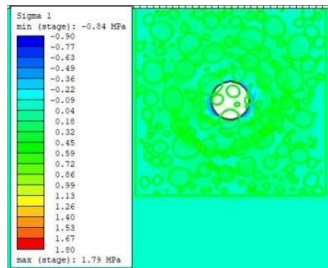


25% - 10

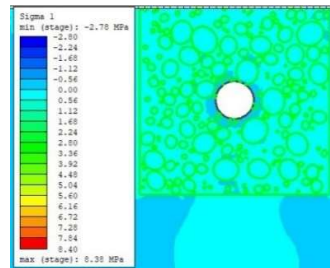
Maximum Stress (σ_1) of VBP 25%



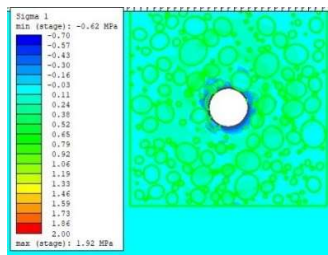
40% - 1



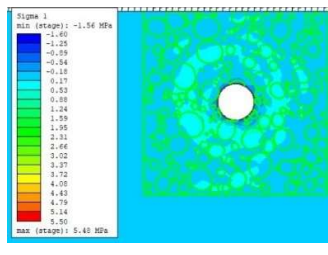
40% - 2



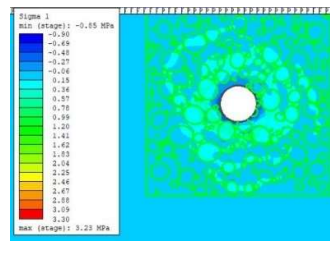
40% - 3



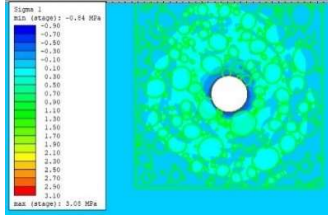
40% - 4



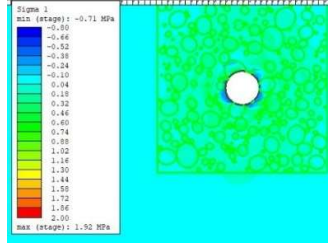
40% - 5



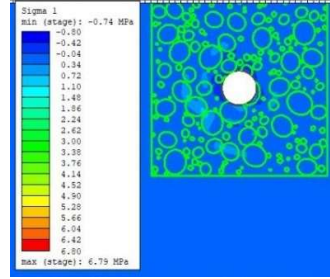
40% - 6



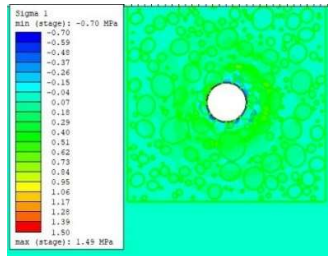
40% - 7



40% - 8

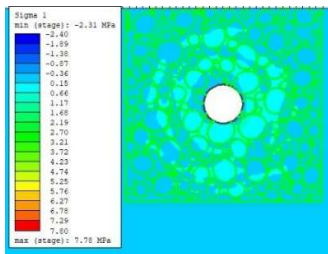


40% - 9

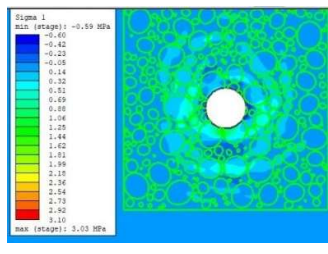


40% - 10

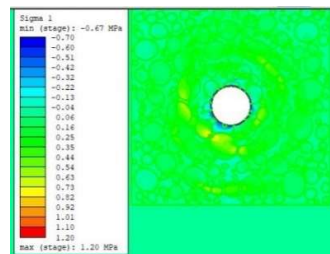
Maximum Stress (σ_1) of 40% VBP



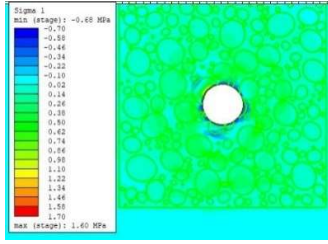
55% - 1



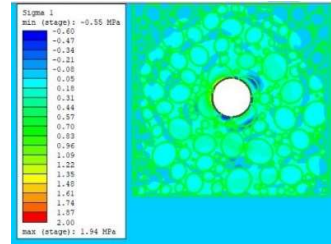
55% - 2



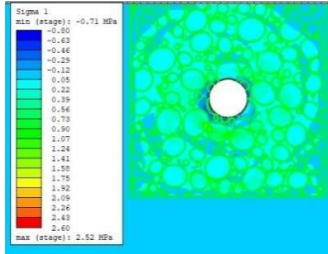
55% - 3



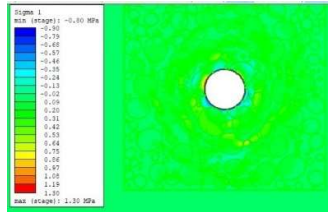
55% - 4



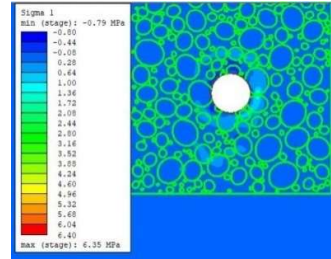
55% - 6



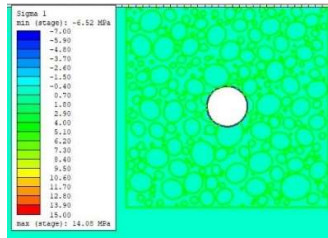
55% - 7



55% - 8



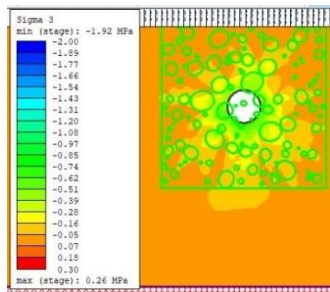
55% - 9



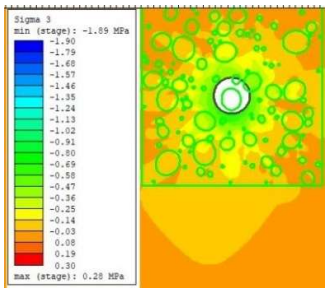
55% - 10

Maximum Stress (σ_1) of 55% VBP

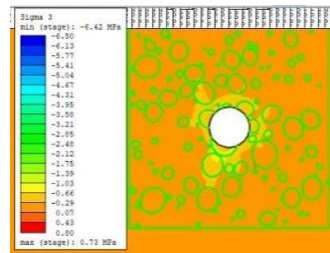
Minimum Stress (σ_3) contours



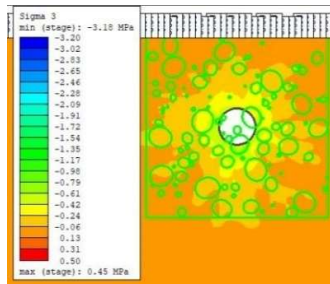
25% - 1



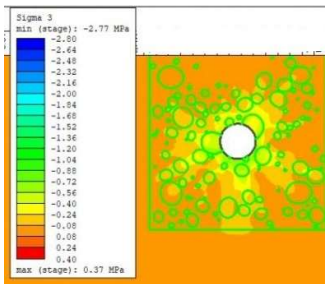
25% - 2



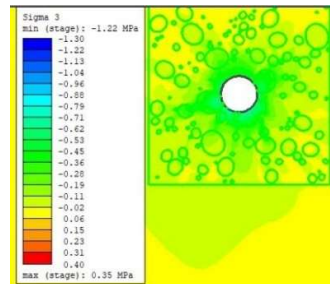
25% - 3



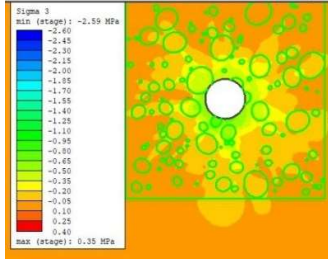
25% - 4



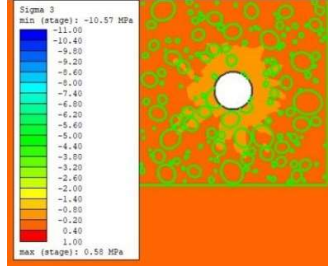
25% - 5



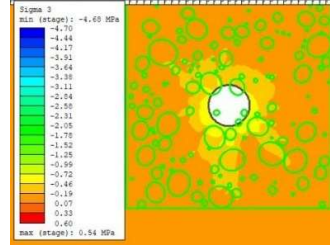
25% - 6



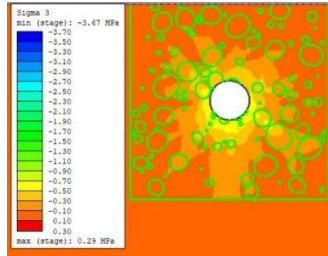
25% - 7



25% - 8

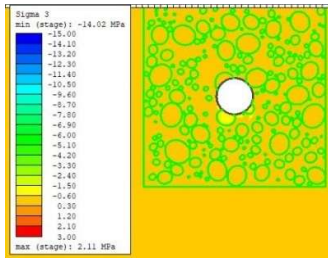


25% - 9

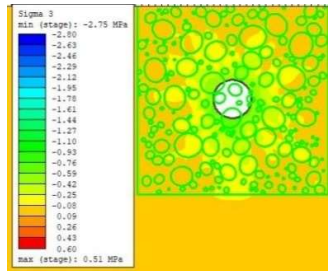


25% - 10

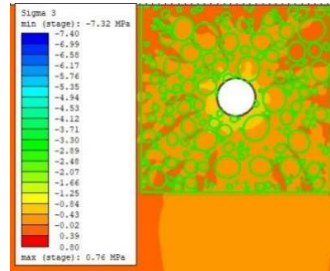
Minimum Stress (σ_3) of 25% VBP



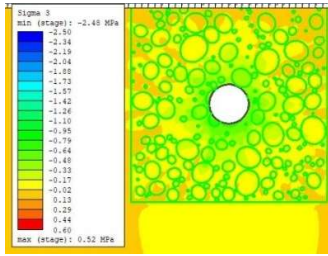
40% - 1



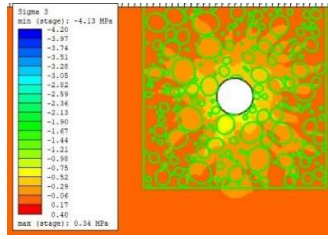
40% - 2



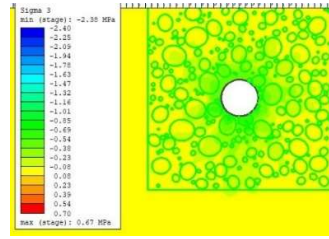
40% - 3



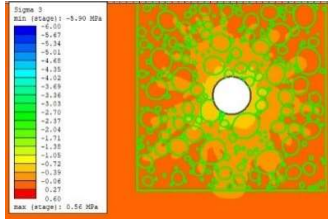
40% - 4



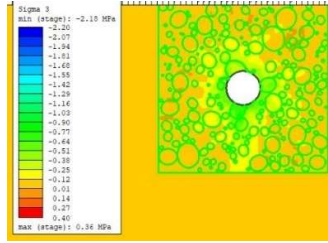
40% - 5



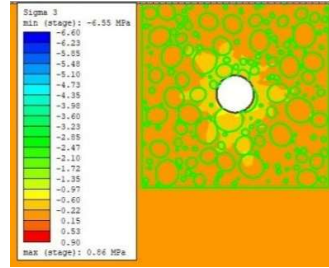
40% - 6



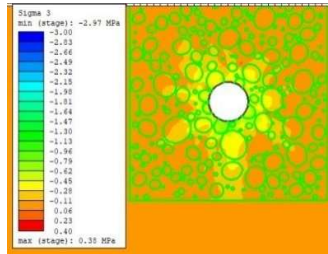
40% - 7



40% - 8

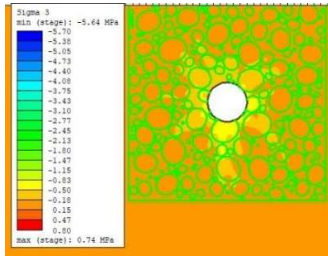


40% - 9

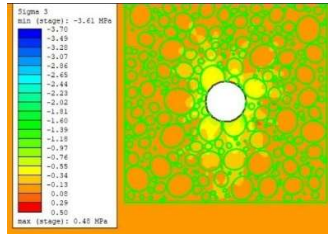


40% - 10

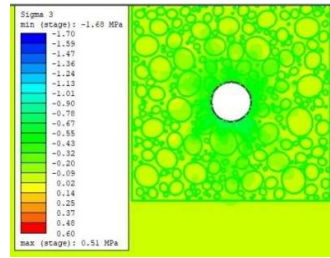
Minimum Stress (σ_3) of 40% VBP



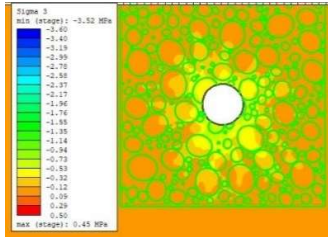
55% - 1



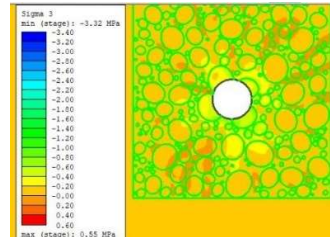
55% - 2



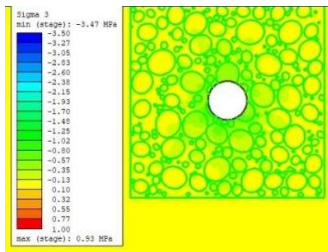
55% - 3



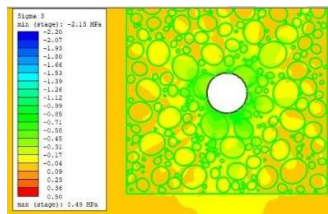
55% - 4



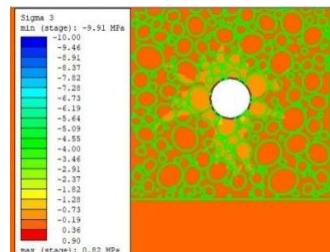
55% - 6



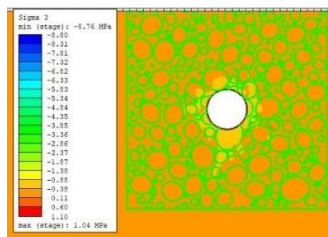
55% - 7



55% - 8



55% - 9



55% - 10

Minimum Stress (σ_3) of 55% VBP

